A Comparative Simulation of Glycerol Steam Reforming with Foam and Conventional Pellet Catalysts in Packed Bed Reactor

Miss Chattharika Phitchayakorn

จุฬาลงกรณ์มหาวิทยาลัย
CHULALONGKORN UNIVERSITY

A Thesis Submitted in Partial Fulfillment of the Requirements
for the Degree of Master of Engineering in Chemical Engineering
Department of Chemical Engineering
FACULTY OF ENGINEERING
Chulalongkorn University
Academic Year 2020

การจำลองปฏิกิริยารีฟอร์มมิงของกลีเซอรอลเชิงเปรียบเทียบด้วยตัวเร่งปฏิกิริยาแบบโฟมและเม็ด
ดั้งเดิมในเครื่องปฏิกรณ์แบบเบดนิ่ง

น.ส.ฉัตรฑริกา พิชญากร

วิทยานิพนธ์นี้เป็นส่วนหนึ่งของการศึกษาตามหลักสูตรปริญญาวิศวกรรมศาสตรมหาบัณฑิต
สาขาวิชาวิศวกรรมเคมี ภาควิชาวิศวกรรมเคมี
คณะวิศวกรรมศาสตร์ จุฬาลงกรณ์มหาวิทยาลัย
ปีการศึกษา 2563
ลิขสิทธิ์ของจุฬาลงกรณ์มหาวิทยาลัย

Thesis Title   A Comparative Simulation of Glycerol Steam Reforming
                      with Foam and Conventional Pellet Catalysts in Packed
                      Bed Reactor
By   Miss Chattharika Phitchayakorn
Field of Study   Chemical Engineering
Thesis Advisor   Professor SUTTICHAI ASSABUMRUNGRAT, Ph.D.
Thesis Co Advisor   Assistant Professor Amata Anantpinijwatna, Ph.D.

Accepted by the FACULTY OF ENGINEERING, Chulalongkorn University in Partial Fulfillment of the Requirement for the Master of Engineering

.... Dean of the FACULTY OF
                                            ENGINEERING
(Professor SUPOT TEACHAVORASINSKUN, D.Eng.)

THESIS COMMITTEE

.... Chairman
(Professor SIRIPORN DAMRONGSAKKUL, Ph.D.)

.... Thesis Advisor
(Professor SUTTICHAI ASSABUMRUNGRAT, Ph.D.)

.... Thesis Co-Advisor
(Assistant Professor Amata Anantpinijwatna, Ph.D.)

.... Examiner
(Assistant Professor PALANG BUMROONGSAKULSAWAT,
Ph.D.)

.... External Examiner
(Assistant Professor Lida Simasatitkul, Ph.D.)

ฉัตรฑริกา พิชญากร : การจำลองปฏิกิริยารีฟอร์มมิงของกลีเซอรอลเชิงเปรียบเทียบด้วยตัวเร่ง
ปฏิกิริยาแบบโฟมและเม็ดดั้งเดิมในเครื่องปฏิกรณ์แบบเบดนิ่ง. (A Comparative
Simulation of Glycerol Steam Reforming with Foam and Conventional Pellet
Catalysts in Packed Bed Reactor) อ.ที่ปรึกษาหลัก : ศ. ดร.สุทธิชัย อัสสะบำรุงรัตน์, อ.ที่
ปรึกษาร่วม : ผศ. ดร.อมตะ อนันต์พินิจวัฒนา

งานวิจัยเรื่องนี้จัดทำขึ้นเพื่อศึกษาการผลกระทบของโครงสร้างของตัวเร่งปฏิกิริยาที่แตกต่าง
กันในเครื่องปฏิกรณ์แบบเบดนิ่งสำหรับกระบวนการผลิตไฮโดรเจนจากปฏิกิริยารีฟอร์มมิ่งของกลีเซอรอล
โดยใช้โปรแกรม COMSOL Multiphysics แบบจำลองเนื้อเดียวเทียมสองมิติที่สภาวะคงที่ของเครื่อง
ปฏิกรณ์ขนาดเส้นผ่านศูนย์กลาง 6 นิ้วได้ถูกสร้างขึ้นเพื่อใช้อธิบายปรากฏการณ์การถ่ายโอนภายในเครื่อง
ปฏิกรณ์ที่มีโครงสร้างของตัวเร่งปฏิกิริยาสองชนิดที่แตกต่างกันได้แก่ (เม็ดดั้งเดิมขนาด 1 นิ้ว และ โฟม
ขนาด 10-30 PPI) จากผลการจำลองพบว่าเครื่องปฏิกรณ์ที่บรรจุตัวเร่งปฏิกิริยาแบบโฟมช่วยปรับปรุง
ประสิทธิภาพของกระบวนการทั้งด้านความดันลด และ ผลได้ไฮโดรเจน เมื่อเทียบกับเครื่องปฏิกรณ์ที่
บรรจุตัวเร่งปฏิกิริยาแบบเม็ดดั้งเดิม โดยที่เครื่องปฏิกรณ์ที่บรรจุตัวเร่งปฏิกิริยาแบบเม็ดดั้งเดิมให้ผลได้
ไฮโดรเจนสูงสุดที่ 55% โดยใช้ความยาวของเครื่องปฏิกรณ์ 15 เมตรในขณะที่เครื่องปฏิกรณ์ที่บรรจุตัวเร่ง
ปฏิกิริยาแบบโฟมให้ผลได้ไฮโดรเจนสูงสุดที่ 60% โดยใช้ความยาวของเครื่องปฏิกรณ์เพียงแค่ 1 ใน 3
ของความยาวที่ใช้ในตัวเร่งปฏิกิริยาแบบเม็ดดั้งเดิม และสามารถลดความดันลดได้ถึง 95% แต่อย่างไรก็
ตามตัวเร่งปฏิกิริยาแบบโฟมได้แสดงการลดลงของอุณหภูมิถึง 15% จากอุณหภูมิเริ่มต้น ในขณะที่ตัวเร่ง
ปฏิกิริยาแบบเม็ดดั้งเดิมแสดงการลดลงของอุณหภูมิเพียง 8% อุณหภูมิที่ลดลงอย่างมากของตัวเร่ง
ปฏิกิริยาแบบโฟมส่งผลต่อสมดุลเคมีโดยเปลี่ยนปฏิกิริยาหลักไปเป็นปฏิกิริยาข้างเคียงและผลิตผลิตภัณฑ์
พลอยได้เพิ่มขึ้น ซึ่งจากผลการศึกษาพบว่าโครงสร้างเซลล์เปิดของตัวเร่งปฏิกิริยาแบบโฟมจะช่วยเพิ่ม
ช่องว่างภายในเครื่องปฏิกรณ์ทำให้ของไหลสามารถไหลได้สะดวก ซึ่งโครงสร้างดังกล่าวช่วยลดการจำกัด
การแพร่ที่พบในกรณีของตัวเร่งปฏิกิริยาแบบเม็ดดั้งเดิมได้อีกด้วย ดังนั้นจากผลการศึกษาจึงพบว่าตัวเร่ง
ปฏิกิริยาแบบโฟมสามารถนำมาใช้แทนที่ตัวเร่งปฏิกิริยาแบบเม็ดดั้งเดิมในเครื่องปฏิกรณ์แบบเบดนิ่งเพื่อ
ช่วยปรับปรุงประสิทธิภาพของกระบวนการผลิตไฮโดรเจนจากปฏิกิริยารีฟอร์มมิ่งของกลีเซอรอลได้

สาขาวิชา	วิศวกรรมเคมี	ลายมือชื่อนิสิต ....
ปีการศึกษา	2563	ลายมือชื่อ อ.ที่ปรึกษาหลัก ....
		ลายมือชื่อ อ.ที่ปรึกษาร่วม ....

6170914921 : MAJOR CHEMICAL ENGINEERING

KEYWORD: Glycerol steam reforming; Computational fluid dynamics; Packed bed reactor; Foam catalyst; Pellet catalyst

Chattharika Phitchayakorn : A Comparative Simulation of Glycerol Steam Reforming with Foam and Conventional Pellet Catalysts in Packed Bed Reactor. Advisor: Prof. SUTTICHAI ASSABUMRUNGRAT, Ph.D. Co-advisor: Asst. Prof. Amata Anantpinijwatna, Ph.D.

This research aimed to study the effect of different catalyst structures to the hydrogen production process with glycerol steam reforming in packed bed reactors via the COMSOL Multiphysics program. 2D pseudo-homogeneous steady-state model of a 6-inch diameter adiabatic reactor has been developed to describe a transport phenomenon inside the packed bed reactors with two different catalyst structures of conventional 1-inch pellet catalyst and 10-30PPI foam catalyst. The simulated results show that the novel foam catalyst improved the process performance in terms of pressure drop and hydrogen yield comparing to the conventional 1-inch pellet catalyst. The reactor packed with the conventional 1-inch pellet catalyst provided the maximum hydrogen yield of 55% at 15 m reactor length, while the novel foam catalyst provided the maximum hydrogen yield of 60% at only one-third of reactor length and reduced 95% of pressure drop. However, the novel foam catalyst exhibited a 15% temperature dropping from its initial temperature, while the conventional pellet catalyst dropped only 8%. The greater temperature dropping of the novel foam catalyst affected the chemical equilibrium by shifting the main reaction to the side reaction and producing more by-products. From the simulation results, the open-cell structure of the novel foam catalyst increases the passage flow of fluid thereby, the diffusion limit of the conventional catalyst has been diminished. The novel foam catalyst can be further used in the packed bed reactor to improve the process performance of the glycerol steam reforming process.

Field of Study:	Chemical Engineering	Student's Signature	....
Academic Year:	2020	Advisor's Signature	....
		Co-advisor's Signature	....

ACKNOWLEDGEMENTS

TABLE OF CONTENTS

LIST OF TABLES

LIST OF FIGURES

จุฬาลงกรณ์มหาวิทยาลัย

CHULALONGKORN UNIVERSITY

CHAPTER 1 INTRODUCTION

1.1 Motivation

Nowadays, global warming becomes a serious problem which affects our communities, our health, and our climate. Human activities that release carbon to the atmosphere are the primary causes of the global warming problem. The combustion of fossil fuels usually uses for transportation, agriculture activity, industrial usage, residential consumption, or electricity generation. The emissions of carbon dioxide (CO_2) from fossil fuel and industrial processes contributed about 78% of the total carbon dioxide emission from 1970 to 2010 [1]. Therefore, the development of sustainable and renewable energy becomes the goal of our study.

Hydrogen is one of the cleaner alternative energies that can replace fossil fuels. It's been used as an alternative fuel for vehicles and industries. Moreover, hydrogen can be used as a raw material in many chemical processes such as the production of green diesel, hydrochloric acid, and other substances. The combustion of hydrogen yields totally non-polluting products and has a high combustion efficiency. Hydrogen production processes mainly comprise water electrolysis, thermochemical process, and biological process [2]. Among these alternatives, the thermochemical process is the most widely used because of its economic advantage, it's proper for a large-scale production, and causes less environmental damage [3]. Several thermochemical hydrogen production technologies have been studied with various types of raw materials, including renewable and non-renewable sources. The reforming of oxygenated hydrocarbons for hydrogen production is one of the most efficient technologies for producing hydrogen from any reactants [4].

Several feedstocks for hydrogen production have been investigated [3]. During the last century, hydrogen was being produced primarily by fossil fuels [5]. However, the fossil fuel pathway has a disadvantage in the carbon dioxide emission that causes global warming. Due to the concern over the global warming issue, the feedstock for the production of hydrogen has been shifted towards cleaner alternatives such as methanol [6], ethanol [7], dimethyl ether (DME) [8], and glycerol [9].

Glycerol ($C_3H_8O_3$) is the main byproduct from the production of biodiesel. Approximately 10% of glycerol is produced for every 100% of biodiesel production [10]. Generally, glycerol from biodiesel production is used in the textile, cosmetics, and food industries. From the year 2000 to 2012, the production of biodiesel increased from about 10 thousand barrels/day to 450 thousand barrels/day, as shown in Figure 1.1 [11]. As a result, glycerol is overproduced for use in those industries, thus the value of glycerol has been continuously decreased. The strategy for the value-adding of glycerol is to convert it into higher-value products such as hydrogen via the steam reforming process [12].
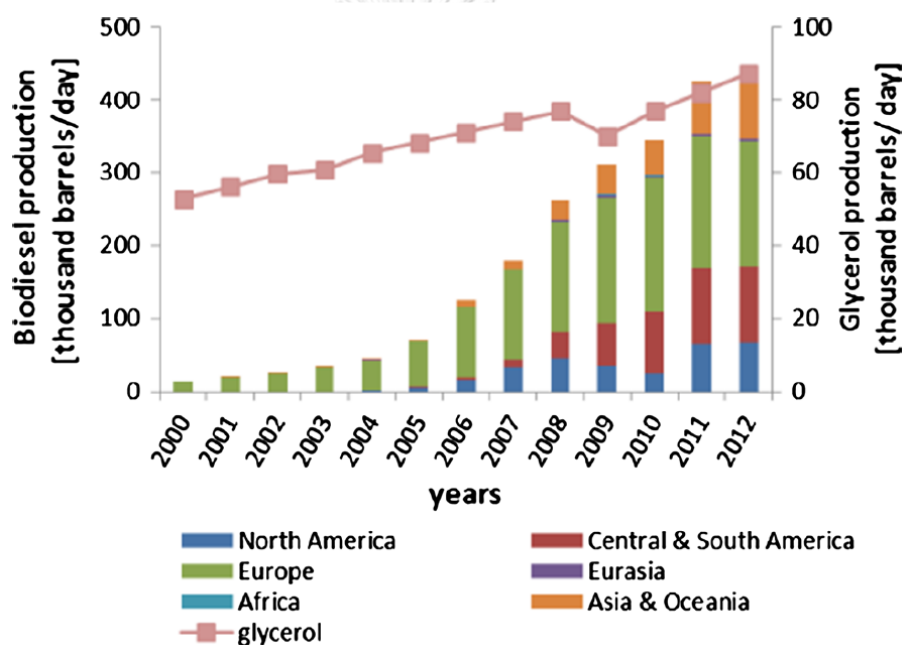
Figure 1.1 Biodiesel and hydrogen production [11]

The glycerol steam reforming reaction commonly operates in a packed bed reactor with a catalytic domain. In heterogeneous catalytic of glycerol steam reforming reaction, Pt, Ni, Ru, Re, Rh, Ir, Co, and Pd were used as catalysts. Among these catalysts, Ni/Al_2O_3 is favorable because of its high catalyst activity and cheapness [12]. The material type of the catalyst is not only significant for the process, but the structure of the catalyst is also important. The modification of catalyst structures was used and explored to optimize reaction, energy, mass, and momentum transfer in the reactor. Several different catalyst structures have been developed, for example, pellet,

powder, monolith, and foams [13]. In a laboratory scale, previous studies [14, 15] used a powder catalyst for the experiment, and some studies [16, 17] investigated the effect of the catalyst structures such as the shape, porosity, and surface area to the hydrogen production efficiency. In an industrial scale, the low ratio between the reactor and particle diameter is used in the packed bed reactor [18]. The pellet catalyst is normally packed in the reactor to achieve this ratio. The pellet catalyst provided a low catalyst activity per unit mass and yielded low conversion because of the difficult diffusion of reactants through the catalyst pore [19]. The powder catalyst was applied to improve the conversion; however, its small particle size led to a large pressure drop across the reactor, which increased the operating cost of the pump or compressor for the operation [20]. The novel structure of foam with an open-cell structure is an alternative to study the improvement of process performance in the reactor.

The present study aimed to simultaneously analyze the reaction and transport phenomena of the system on an industrial scale using CFD technique. COMSOL Multiphysics software is used to simulate the glycerol steam reforming process in the reactor packed with the different catalyst structures. The goal of this study is to compare the hydrogen production performance between two different catalyst structures of pellet (1-inch spherical shape) and foam (10-30PPI) and illustrate and validate the effect of the catalyst structure using the CFD technique.

1.2 Research objectives

1.2.1   To simulate glycerol steam reforming with novel foam catalyst and conventional pellet catalyst in packed bed reactor for hydrogen production

1.2.2   To study the effect of catalyst structure on glycerol steam reforming in packed bed reactor.

1.3 Scope of work

      1.3.1   Simulate the two-dimensional steady state pseudo homogeneous packed bed reactor by COMSOL Multiphysics version 5.3a program.

      1.3.2   Validate the kinetic model for glycerol steam reforming in 2 case of catalyst structures:

          -   conventional pellet catalyst (1-inch spherical shape)

          -   novel foam catalyst (10-30PPI foam)

      using Computational Fluid Dynamics (CFD) simulations,

      1.3.3   Investigate the effect of different catalyst structures on the performance of hydrogen production in packed bed reactor.

1.4 Expected benefits

      Find the suitable catalyst structure for improvement the hydrogen production between conventional pellet catalyst and novel foam catalyst in the packed bed reactor.

จุฬาลงกรณ์มหาวิทยาลัย

CHULALONGKORN UNIVERSITY

CHAPTER 2 FUNDAMENTAL AND LITERATURE REVIEWS

This chapter collects and describes information involved in this thesis, including the subjects of hydrogen production, glycerol steam reforming process, nature of packed bed reactor, characteristic of catalyst structure, kinetic modeling, computational fluid dynamics modeling, and literature review of previous model results by comparing between the conventional pellet catalyst and the novel foam catalyst.

2.1. Hydrogen production

Hydrogen is the simplest element on earth, but it's rarely found in the pure form, wherein the physical and chemical properties are following in Table 2.1.

Table 2.1 The basic and chemical properties of hydrogen [21]

Properties of hydrogen molecule	
Formula	H_2
Chemical structure	H-H
Molecular weight	2.0159
Appearance	Colorless and odorless gas at room temperature
Density (gas)	0.08988 gL^{-1} (0 °C, 1 atm)
Relative vapor density (air = 1)	0.07
Density (liquid)	70.8 gL^{-1} (at -253 °C)
Melting point	-259.35 °C
Boiling point	-252.88 °C (at 1 atm)
Solubility in water	0.0214 cm^3g^{-1} (0 °C, 1 atm)
Energy content for 1 kg hydrogen (when reacting with oxygen to form water)	
Higher heating value	141,900 kJ; 33,900 kcal; 39.4 kWh
Lower heating value	120,000 kJ; 28,680 kcal; 32.9 kWh

Hydrogen is versatile and uses in many applications such as feedstocks in chemical processes, energy carrier in transportation, the gas industry, and electricity or

heat generation. More than 80% of the hydrogen produced today is used as feedstocks to make ammonia, fertilizer, and to remove sulfur from fuel in oil refining. Only 1% is used as an energy carrier, to launch satellites and rockets in the space industry [22]. Therefore, the increase in hydrogen production enhances the probability of hydrogen utilization in the future.

Hydrogen can produce from several processes such as electrolysis, biochemical, and thermochemical, as shown in Figure 2.1 [2]. Although the production of hydrogen via the biochemical process consumes less energy, it produces wastewater as a byproduct. The electrolysis of water produces high purity hydrogen without any waste generated, but this process only uses in the special case because of its infeasible economically in the industrial scale. Therefore, the thermochemical process widely uses for hydrogen production because of its more efficient, suitable for large-scale production and less environment damage [3].
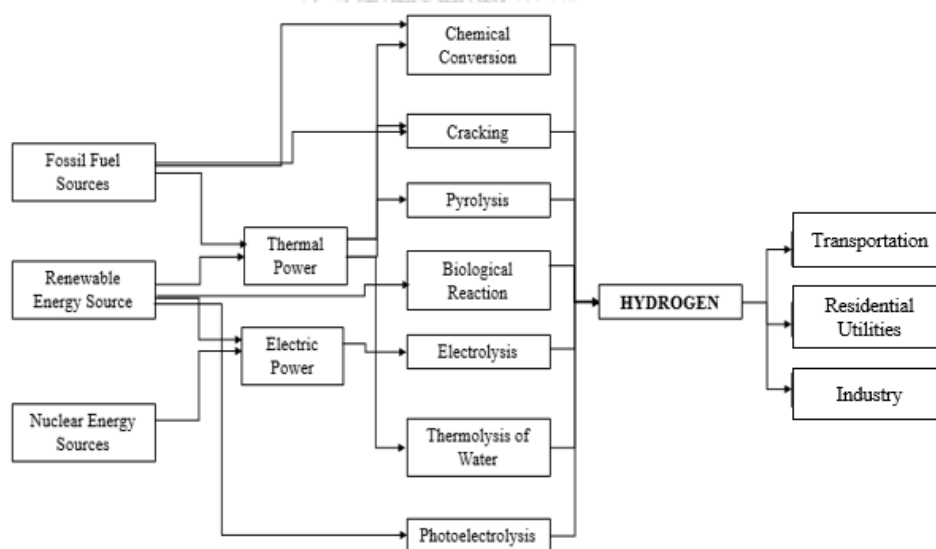
Figure 2.1 Pathways to hydrogen production and utilization [2]

Nowadays, most hydrogen productions are mainly produced from fossil fuel, but the concerning over global warming issues has been shifted towards the feedstocks to produce hydrogen to be cleaner alternatives. Several renewable compounds such

as (glycerol, methanol, and ethanol) can be transformed into hydrogen form from the above processes.

2.2 Glycerol steam reforming process (GSR)

The production of biodiesel is continuously grown in recent years. The biodiesel production process consists of transesterification oil-containing raw materials such as soybean, rapeseed, and sunflower oils. This process produces biodiesel as a main product and glycerol as the main byproduct, as shown in Figure 2.2. Approximately 10% of glycerol is produced from the biodiesel process [7].
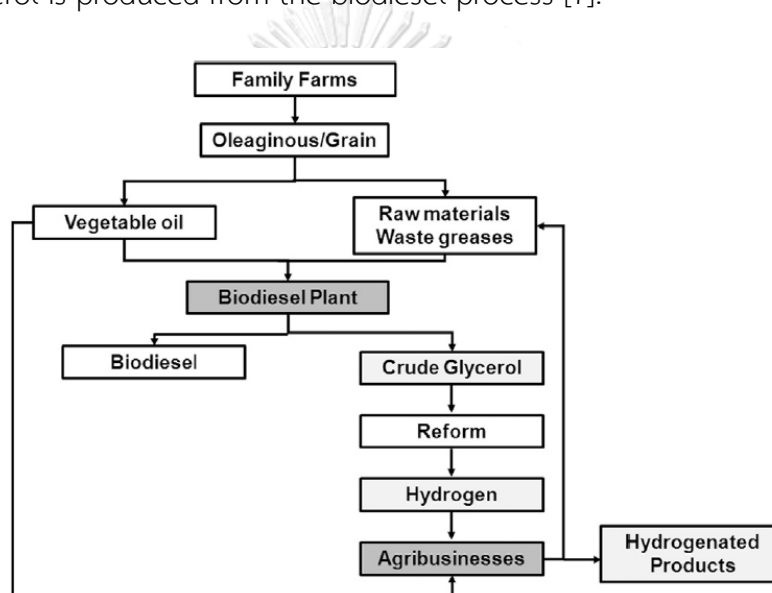
Figure 2.2 Example of the interaction of biodiesel plants and agribusinesses with hydrogen [12]

Glycerol is used as the feedstock in many industrial fields such as pharmaceutics, cosmetics, personal care products, resins, plastic, and detergents. Glycerol ($C_3H_8O_3$) is also knowns as 1,2,3-propane tri-ol or glycerine [23]. The chemical structure is shown in Figure 2.3: and the properties of glycerol are shown in Table 2.2.
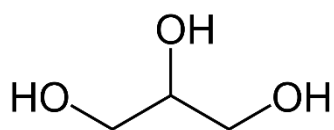
Figure 2.3 Chemical structure of glycerol [23]

Table 2.2 The properties of glycerol compound [24]

Properties of glycerol compound	
Formula	$C_3H_8O_3$
Molecular Weight	92.09 g/mol
Appearance	Colorless to brown colored liquid and odorless
Density	1.2613 gL^{-1} (at 68 °F)
Flash point	177 °C
Melting point	18.2 °C
Boiling point	290.0 °C (at 1 atm)
Solubility in water	500 gL^{-1} (at 20 °C)
Vapor pressure	< 1 mm Hg (at 20 °C)
Form	Viscous liquid
Color	APHA: ≤10
Explosive limit	2.6 – 11.3 %

Stream reforming is commonly used in the thermochemical processes to produce hydrogen from fossil fuels or renewable fuels such as glycerol. In GSR process, glycerol reacts with steam in the presence of catalysts, and produces hydrogen, carbon dioxide, and carbon monoxide. The overall reaction of the GSR process presents as the sum between two reactions of glycerol decomposition reaction and water-gas shift reaction as shown in Eq. 2.1.

$$C_3H_8O_3 + 3H_2O \rightarrow 7H_2 + 3CO_2 \qquad (\Delta H_r^0 = +128 \text{ kJ/mol}) \qquad \text{(Eq. 2.1)}$$
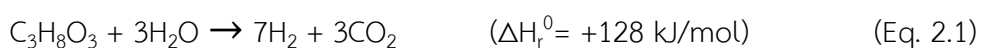
Generally, the reactions of the GSR process involve 2 main reactions (glycerol decomposition and water-gas shift) and 2 side reactions (CO-methanation and coke formation), as shown in Eq. 2.2 – 2.5 [12].

- Glycerol decomposition

$$C_3H_8O_3 \longrightarrow 3CO + 4H_2 \qquad (\Delta H_r^0 = +251 \text{ kJ/mol}) \qquad \text{(Eq. 2.2)}$$

- Water-gas shift

$$CO + H_2O \rightleftharpoons H_2 + CO_2 \qquad (\Delta H_r^0 = -41 \text{ kJ/mol}) \qquad \text{(Eq. 2.3)}$$

- CO-Methanation

$$CO + 3H_2 \rightleftharpoons CH_4 + H_2O \qquad (\Delta H_r^0 = -206 \text{ kJ/mol}) \qquad \text{(Eq. 2.4)}$$

- Coke formation

$$H_2 + CO \rightleftharpoons C + H_2O \qquad (\Delta H_r^0 = -131 \text{ kJ/mol}) \qquad \text{(Eq. 2.5)}$$
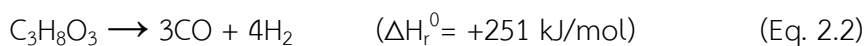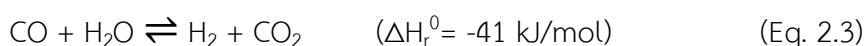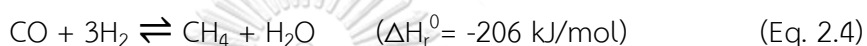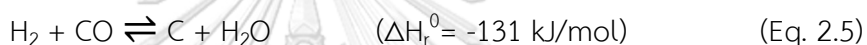
2.2.1 Process operating condition

Many researchers have been studied to find the suitable operating condition for the GSR process by varying temperature, pressure, and water to glycerol feed ratio (WGFR).

- **Temperature**

The temperatures were studied to find the proper ranges that gave the highest glycerol conversion. According to the high positive enthalpy of the overall reaction in Eq. 2.1, the GSR reaction performs as an endothermic behavior that requires an external heat to convert the glycerol into synthesis gas. As shown in Figure 2.4, hydrogen yield increased with the temperature raised and beyond an optimum temperature. The favorable temperatures for the GSR process are in the range of 823 - 923 K. Above the temperature of 923 K, the hydrogen yield continuously decreased because at this point the catalyst was deactivated and lost the reaction area [25].

• **Pressure**

According to the thermodynamic analysis, the optimal pressure for hydrogen production is operated at atmospheric condition [26]. In an ideal case, a vacuum pressure can improve the operation of hydrogen production because this condition reduced the reacting temperature, energy consumption, and catalyst deactivation [27]. But in the real operation, the use of vacuum pressure will enhance the operating cost of pump working and the use of atmospheric pressure must be favorable.
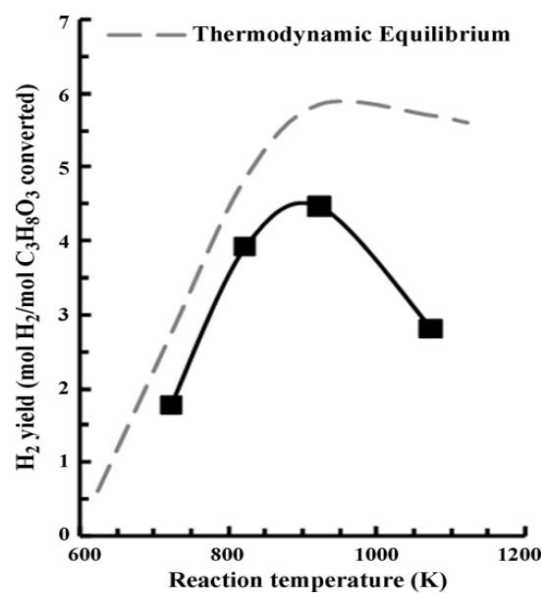
Figure 2.4 Hydrogen yield (mol of hydrogen produced per mol of glycerol converted) vs temperature on Rh/Al$_2$O$_3$ catalyst. GHSV= 30,000 h$-$1; WGR = 3 mol/mol. [25]

• **Water to glycerol feed ratio (WGFR)**

The water to glycerol feed ratio strongly influences the yield and selectivity of hydrogen production. From Le Chatelier's Principle, at high water to glycerol feed ratio, the equilibrium will shift towards the excess water consumption and producing more hydrogen [27]. As shown in Figure 2.5, the most favorable ratio is 9:1 and above this ratio the hydrogen yield slowly increases. Moreover, at the high WGFR, the coke formation reaction is neglected because of the limiting of glycerol reactant [28].
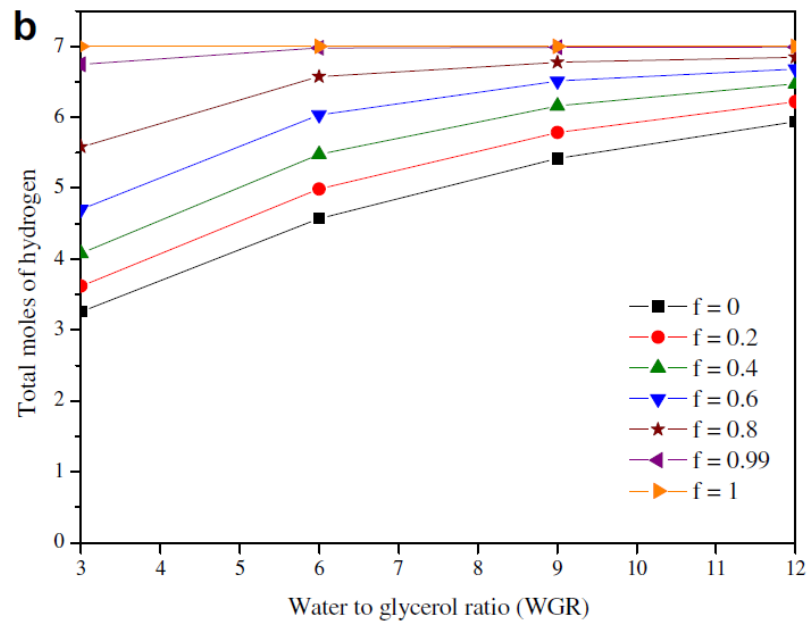
Figure 2.5 Thermodynamic investigation of hydrogen production: effects of WGR at temperature (850 K), atmospheric pressure (f is hydrogen fraction removal) [27]

2.3 Packed bed reactor

A packed bed reactor commonly uses in the heterogeneous catalytic process because of its economic efficiency. In basic design, a column fills with catalyst particles, and these particles can create with various structures. The main advantage of the packed bed reactor is the high conversion rate per weight of catalyst.

The structure of the catalyst particles makes the modeling of mass and energy transport in the packed bed reactor, whereas the chemical reaction occurs on the surface of the catalyst. The heterogeneous catalytic reaction involves the following 7 steps as shown in Figure 2.6 [29], where each steps are explained below [30]:

1. Diffusion of the reactants from the bulk fluid to the external surface of the catalyst pellet
2. Diffusion of the reactants through catalyst pores
3. Adsorption of the reactants onto the catalyst surface inside pores
4. Reaction on the catalyst surface
5. Desorption of the products from catalyst surface

6. Diffusion of the products from inside catalyst pores to catalyst surface

7. Diffusion of the products from surface of the catalyst pellet to the bulk fluid
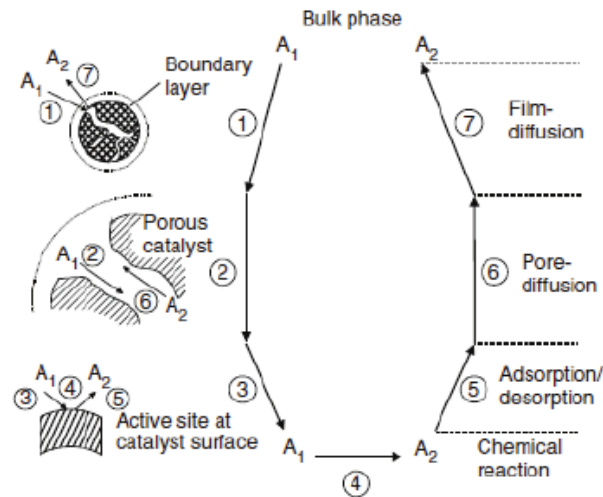
Figure 2.6 The heterogeneous catalytic steps for catalytic fluid–solid reaction
A1 ⟶ A2 on a catalyst media [29]

2.4 Catalyst structure

Catalysts are chemical species that decrease the activation energy and increase the rate of a chemical reaction. Various catalyst structures have been developed to improve the reaction performance. The important properties of catalyst structure to achieve high product yield are large surface area, good mechanical strength, high activity, high coefficient of heat transfer, high coking resistance, and high permeability for flowing of the reactants [31]. The examples of catalyst structure are pellet, powder, monolith, and foams.

Nowadays, the widespread study of novel catalyst structures to replace the conventional catalyst structure becomes attentions. Most studies applied the pellet or the monolith structure to use in the packed bed reactor [13], and less study used the foam structure. The application of the novel foam structure is one of the interesting structures to compare the performance of the packed bed reactor with the conventional one.

2.4.1 Conventional pellet catalyst

In the industrial scale, the catalyst structure in the packed bed reactor commonly uses the large size of pellet structure to maintain the low ratio between the reactor and particle diameter [18], wherein the catalyst pellets hold inside the bed and do not move during the operation, as shown in Figure 2.7. The conventional pellet catalyst has fine pores at the outer surface for accessibility of the reactants inside the structure. Because of the difficult accessibility of the reactants through very fine pores, the design towards smaller particles to obtain a larger specific surface area and rises to maximum reaction rate. However, the use of small catalyst particles leads to a large pressure drop and contrary affecting the operating cost of the pump working [20].
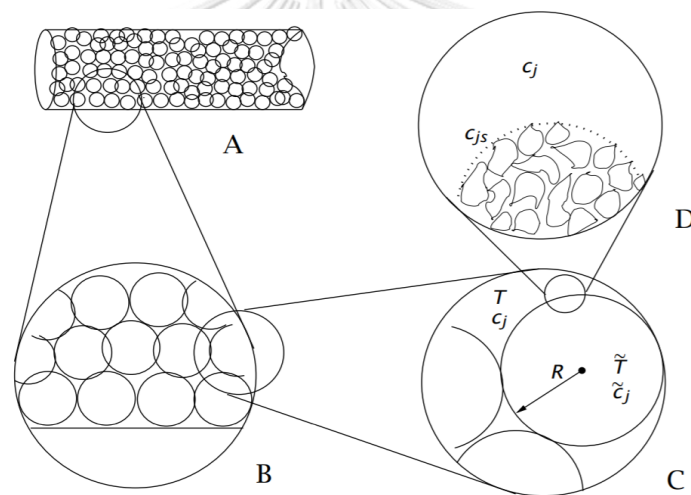
Figure 2.7 Conventional spherical catalyst pellets [20]

2.4.2 Novel foam catalyst

The novel structure of foam catalysts for improving the process performances has been presented. Foam structures characterizes as "closed–cell" and "open-cell", the two characterizations have different properties and structures. The closed-cell structure has the form of no interconnectivity between cells, while the open-cell structure has the form of interconnectivity between cells to allow the flowing of fluid. The open-cell structure is widely used and applied to be the catalytic domains. The open-cell structure is shown in Figure 2.8, comprising three main components: struts,

which are composed of solid material; cells which are approximately spherical voids enclosed by struts; and windows, which are opening and connecting the cells [32].
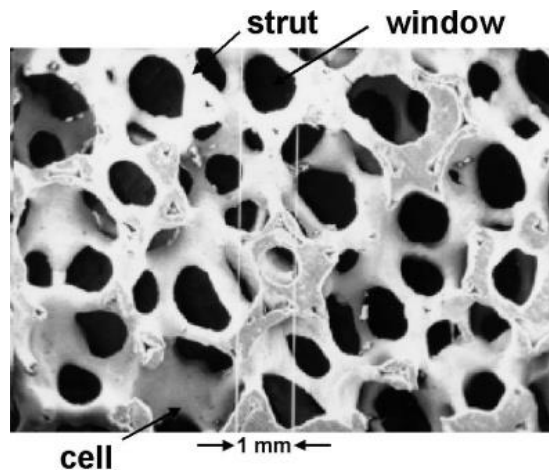
Figure 2.8 Open-cell foam structure [32]

In comparison, the obviously different parameters between the pellet and foam catalyst are open porosity in the packed bed reactor. Normally, the porosity ranges of the conventional pellet catalyst are 0.2 to 0.4, based on the different shapes and structures, while the foam catalyst has the porosity more than 0.8 according to the open-cell structure.

2.5 Kinetic Modeling

In simulation, the kinetic modeling is an important point to present the reaction of process. Many studies have been investigated the kinetic modeling of the GSR process using different catalysts.

Adhikari, S. et al. (2009) kinetic modeling

Adhikari, S. et al. [33] compared the different supported catalysts of CeO_2-, MgO-, and TiO_2- in the GSR process. From the study, Ni catalyst with CeO_2- support performed the best performance. As shown in Eq. 2.6, the kinetic modeling of this study performed only the glycerol changes because the concentration of water was presented in excess compared to the concentration of glycerol. The other kinetic parameters are shown in Table 2.3.

$$R = k_0 \exp^{-Ea/RT} [C_{glycerol}]^{0.233} \qquad \text{(Eq. 2.6)}$$

The average deviation between the experimental conversion and the model-predicted values was 6.7%, as shown in Figure 2.9.
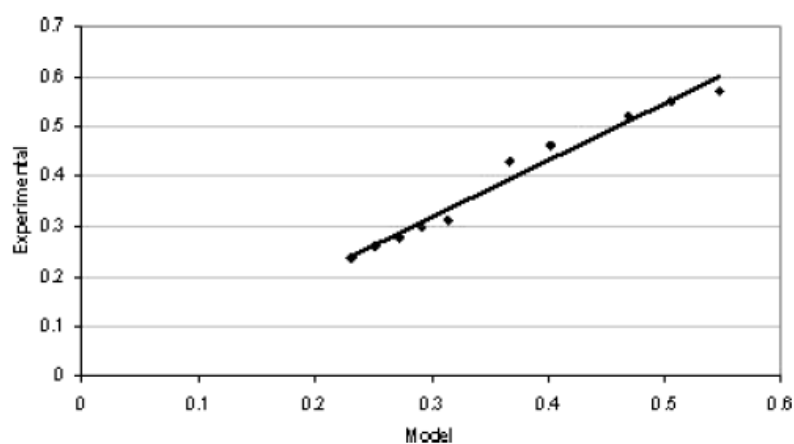
Figure 2.9 The comparison between experimental and model predicted of glycerol conversion [33]

Cheng, C.K. et al. (2010) kinetic modeling

Cheng, C.K. et al. [34] used a bimetallic Co-Ni/Al$_2$O$_3$ catalyst to investigate the catalyst activity in the GSR process and compared with other catalysts. The reaction study over Co-Ni/Al$_2$O$_3$ presented the kinetic rate in both the Power-law and Langmuir-Hinshelwood form for representing the summation of the glycerol decomposition and water-gas shift reaction. The Power-law model of this study referred to the parameter of glycerol consumption and product generation such as CO$_2$, H$_2$, CO, and CH$_4$ [34], as shown in Eq. 2.7. The constant values of the kinetic parameters are shown in Table 2.3.

$$R_i = k_0 \exp^{(-Ea/RT)} p_{C_3H_8O_3}^{0.253} p_{H_2O}^{0.358} \qquad \text{(Eq. 2.7)}$$

Moreover, Langmuir-Hinshelwood model described the adsorption of glycerol and steam on the catalytic domains. The model depended on the partial pressure of glycerol and steam. As a result, it seems that the GSR process on the Co-Ni/Al$_2$O$_3$

catalyst proceeded via a dual-site mechanism involving molecular adsorption of both reactants, as shown in Eq. 2.8. The kinetic parameters are shown in Table 2.3.

$$R_{GSR} = \frac{k_0 p_{C_3H_8O_3} p_{H_2O}}{(1 + K_{C_3H_8O_3} p_{C_3H_8O_3})(1 + K_{H_2O} p_{H_2O})} \qquad \text{(Eq. 2.8)}$$

From the estimation of the kinetic modeling, the parity of model predictions was similar to the experimental, as shown in Figure 2.10.
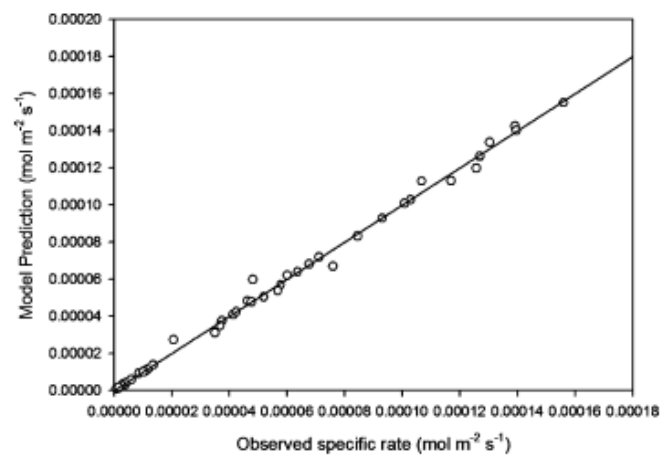
Figure 2.10 Parity plot showing comparison between predicted and measured formation rates for H_2, CO_2, CO, and CH_4 [34]

Nor Shahirah, M.N., et al. (2016) kinetic modeling

Nor Shahirah, M.N., et al. [35] studied the kinetics of GSR process over Ni/Al_2O_3 catalyst, as shown in Eq. 2.9-2.10. This study revealed only the power-law model of the glycerol decomposition reaction and did not show other side reactions. The other kinetic parameters are shown in Table 2.3.

$$R_{glycerol-decomposition} = k_{glycerol-decomposition} p_{C_3H_8O_3}^{1.2} \qquad \text{(Eq. 2.9)}$$

$$k_{glycerol-decomposition} = k_0 \exp\left(\frac{-Ea}{RT}\right) \qquad \text{(Eq. 2.10)}$$

Abbas, S.Z. et al. (2017) kinetic modeling

Abbas, S.Z. et al. [26] studied the kinetic modeling of other side reactions of the water-gas shift and CO-methanation reaction with respect to the Ni/Al_2O_3 catalyst. The complex form of the Langmuir-Hinshelwood model was expressed in Eq. 2.11-2.12. Moreover, the auxiliary equation and the kinetic parameters constant are shown in Eq. 2.13-2.16, and Table 2.3, respectively.

Water-gas shift:

$$R_{water-gas-shift} = \frac{k_{water-gas-shift}}{p_{H_2}} \left(p_{CO}p_{H_2O} - \frac{p_{H_2}p_{CO_2}}{K_{water-gas-shift}} \right) \left(\frac{1}{\Omega^2} \right) \qquad \text{(Eq. 2.11)}$$

CO-methanation:

$$R_{CO-methanation} = \frac{k_{CO-methanation}}{p_{H_2}^{2.5}} \left(\frac{p_{H_2}^2 p_{CO}}{K_{CO-methanation}} - p_{CH_4}p_{H_2O} \right) \left(\frac{1}{\Omega^2} \right) \qquad \text{(Eq. 2.12)}$$

$$k_{water-gas-shift/CO-methanation} = k_0 \exp\left(\frac{-Ea_{water-gas-shift/CO-methanation}}{RT} \right) \qquad \text{(Eq. 2.13)}$$

$$K_{water-gas-shift} = \exp\left(\frac{4400}{T} - 4.036 \right) \qquad \text{(Eq. 2.14)}$$

$$K_{CO-methanation} = \exp\left(-\frac{26830}{T} + 30.114 \right) \qquad \text{(Eq. 2.15)}$$

$$\Omega = 1 + K_{CO}p_{CO} + K_{H_2}p_{H_2} + K_{CH_4}p_{CH_4} + K_{H_2O}\frac{p_{H_2O}}{p_{H_2}} \qquad \text{(Eq. 2.16)}$$

Table 2.3 Summary of kinetic modeling parameter of glycerol steam reforming reaction from previous studied

Study	Parameter	Value	Unit
Adhikari, S. et al. [33] • Ni/CeO$_2$ • 873-923 K	k_0 Ea	8135.5 103.4	$kmol^{0.767}/s^{0.767}kg_{cat}$ kJ/mol
Cheng, C.K. et al. [34] Power law model • Co-Ni/Al$_2$O$_3$ • 773-823 K	k_0 Ea	0.036 63.30	$mol \cdot m^{-2} \cdot s^{-1} \cdot kPa^{-0.611}$ kJ/mol
Cheng, C.K. et al. [34] LH model • Co-Ni/Al$_2$O$_3$ • 773-823 K	k_0 K_{C3H8O3} K_{H2O}	5.570×10^{-7} 0.2830 0.0369	$mol \cdot m^{-2} \cdot s^{-1} \cdot kPa^{-2}$ kPa^{-1} kPa^{-1}
Nor Shahirah, M.N., et al. [35] • Ni/Al$_2$O$_3$ • 823-1073 K	k_0 Ea	3.483×10^{-3} 35.80	$molkPa^{-1.2}m^{-2}s^{-1}$ kJ/mol
Abbas, S.Z. et al. [26] • Ni/Al$_2$O$_3$ • 573-973 K	$k_{0, \text{water-gas-shift}}$ $k_{0, \text{CO-methanation}}$ $Ea_{\text{water-gas-shift}}$ $Ea_{\text{CO-methanation}}$	5.84×10^{-1} 1.258×10^{12} 89.23 257.01	$molkPa^{-1}m^{-2}s^{-1}$ $molkPa^{0.5}m^{-2}s^{-1}$ kJ/mol kJ/mol

2.6 Computational fluid dynamics modeling

The computational fluid dynamics (CFD) is a tool that used to describe a transport phenomenon and apply to a wide range of research and engineering problems. The CFD uses numerical analysis and data structures to analyze and solve problems that involve fluid flows. The CFD uses in many fields of study such as aerodynamics analysis, weather simulation, natural science and environmental engineering, industrial design and analysis, biological engineering and fluid flows, and engine and combustion analysis [36].

The CFD modeling commonly uses to describe the mass transfer, momentum transfer, energy transfer, and chemical or physical phenomena inside the reactor. In order to obtain an approximate solution in CFD modeling, discretization of the partial differential equations to a system of algebraic equations has been done using finite element analysis. The method breaks the domain into many small elements and uses a solver for the approximate solution of each element.

COMSOL Multiphysics is one of the examples of CFD modeling software for modeling and solving all kinds of scientific and engineering problems based on partial differential equations (PDEs). COMSOL Multiphysics is an interactive software with Graphical User Interface (GUI) and finite element method to solve the problems. The software is a simulation platform that encompasses all of the steps in the modeling workflow by defining geometries, appropriate boundary conditions, material properties, and other quantities to describe phenomena and solving or predicting the system [37].

The CFD analysis framework composes of three main elements: pre-processor, solver, and post-processor as shown in Figure 2.11. The pre-processor is an input of the system by composing geometry creation, mesh generation, specification of physical and chemical properties, and definition of the boundary conditions. The solver is a step for applied the boundary condition and transport equations to solve the problems. The post-processor is a step for reported the results from the solver. Moreover, the results from the solver were validated with the experimental data for confirmation of the CFD simulation results.
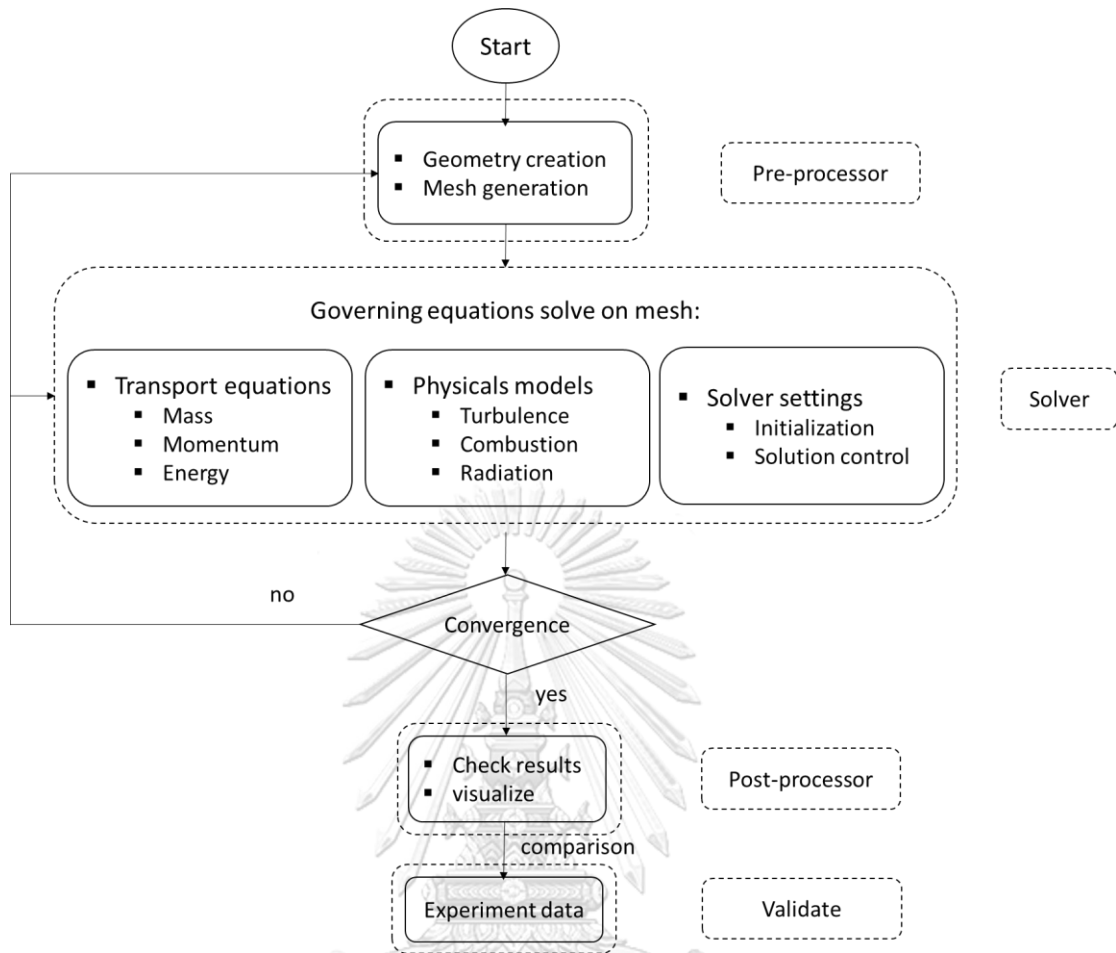
Figure 2.11 CFD analysis framework

2.6.1 Governing equations

The mathematical models for computational fluid dynamics study include fluid flow, chemical reaction, mass, and heat transfer to describe phenomena in both fluid and catalyst phases. The fundamental governing equations are the conservation of mass, momentum, energy, and chemical species.

Conservation of mass:

The conservation of mass is usually expressed using the continuity equation, given in differential form as following:

$$\frac{\partial \rho_f}{\partial t} + \nabla \cdot \left(\rho_f u \right) = 0 \qquad \text{(Eq. 2.17)}$$

This equation validly uses for both compressible and incompressible flows. If the system operates under a steady state condition, the term of $\partial\rho_f/\partial t$ will neglect.

Conservation of momentum:

The conservation of momentum is implied by Newton's laws of motion, given in differential form as following:

$$\frac{\partial(\rho_f u)}{\partial t} + \nabla \cdot \left(\rho_f uu + P - \tau_{stress}\right) + F = 0 \qquad \text{(Eq. 2.18)}$$

The example of an external force (F) is the gravitational body force in the flow direction.

A general form of Newton's law of viscosity uses as the equation to calculate the shear stress (τ_{stress}), as following the equation below:

$$\tau_{stress} = -\mu\left(\nabla u + \left(\nabla u\right)^{T}\right) + \left(\frac{2}{3}\mu - \kappa\right)(\nabla \cdot u)\delta \qquad \text{(Eq. 2.19)}$$

Conservation of energy:

The conservation equation for energy given in differential form as following:

$$\frac{\rho_f C_{p,f} DT}{Dt} = -(\nabla \cdot q) - \left(\tau_{stress} : \nabla \cdot u\right) - \left(\frac{\partial \ln\rho_f}{\partial \ln T}\right)_p \frac{DP}{Dt} + Q_{sv} \qquad \text{(Eq. 2.20)}$$

Conservation of chemical species:

The conservation equation for chemical species given in differential form as following:

$$\frac{\partial c_i}{\partial t} + \nabla \cdot \left(c_i u\right) + \left(\nabla \cdot J_i\right) = R_i \qquad \text{(Eq. 2.21)}$$

The molar diffusion flux (J_i) of species i calculates using a Fick's law, given in differential form as following:

$$J_i = D_i^m \nabla C_i \qquad \text{(Eq. 2.22)}$$

The diffusion coefficient (D_i^m) is calculated by using the mixture of average diffusion model (Eq. 2.24) and the binary diffusion coefficient (D_{ik}) that determined from Fuller equation (Eq. 2.23).

The binary diffusion coefficient (D_{ik}) from Fuller correlation is following below equation:

$$D_{ik} = \frac{10^{-3} T^{1.75} \left(\dfrac{1}{Mw_i} + \dfrac{1}{Mw_k} \right)^{\frac{1}{2}}}{P \left[\left(\sum v_i \right)^{\frac{1}{3}} + \left(\sum v_k \right)^{\frac{1}{3}} \right]^2} \qquad \text{(Eq. 2.23)}$$

where sum of the diffusion volume of component i or k ($\sum v_i$ or $\sum v_k$) can calculate using the sum of atomic diffusion volume as shown in Table 2.4.

Later, the Stefan-Maxwell diffusion equations provided an approximate solution to convert the binary diffusion coefficient (D_{ik}) to the diffusion coefficient (D_i^m) of each species in a mixture as following:

$$D_i^m = \frac{1 - y_i}{\displaystyle\sum_{k \neq i} \frac{y_i}{D_{ik}}} \qquad \text{(Eq. 2.24)}$$

According to the fluid flow in packed bed reactor, an effective diffusion coefficient ($D_{eff,i}$) is one of the important parameter to describe the average diffusion taking place in the catalyst phase as following:

$$D_{eff,i} = \frac{\varepsilon_p}{\tau} \left(\frac{D_i^m D_{KA,i}}{D_i^m + D_{KA,i}} \right) \qquad \text{(Eq. 2.25)}$$

The Knudsen diffusivity ($D_{KA,i}$) was calculated by using below equation:

$$D_{KA,i} = 4850d_{por}\sqrt{\frac{T}{Mw_i}}$$ (Eq. 2.26)

Table 2.4 The values of atomic and simple molecular diffusion volumes[38]

Atomic and structural diffusion volume increments			
C	16.5	(Cl)	19.5
H	1.98	(S)	17.0
O	5.48	Aromatic or heterocyclic rings	-20.2
(N)[a]	5.69		
Diffusion volumes of simple molecules			
H_2	7.07	CO_2	26.9
D_2	6.70	N_2O	35.9
He	2.88	NH_3	14.9
N_2	17.9	H_2O	12.7
O_2	16.6	(CCl_2F_2)	114.8
Air	20.1	(SF_6)	69.7
Ne	5.59	(Cl_2)	37.7
Ar	16.1	(Br_2)	67.2
Kr	22.8	(SO_2)	41.1
(Xe)	37.9		
CO	18.9		

[a]Parentheses indicate that the value is based on only a few data points.

Source: E. N. Fuller, F. D. Schettler, and J. C. Giddings, Ind. Eng. Chem., 58(5), 19 (1966).

2.6.2 Algorithm for finding the solution

A mathematical model of COMSOL Multiphysics software defines based on the finite element method. The finite element method is an engineering tool to understand, predict, and optimize the design or operation of a device or process. This method divides the problem domain into several elements, as shown in Figure 2.12. Then the partial differential equations (PDEs) of each physical law and an algorithm were applied to find the solution of each element [39].
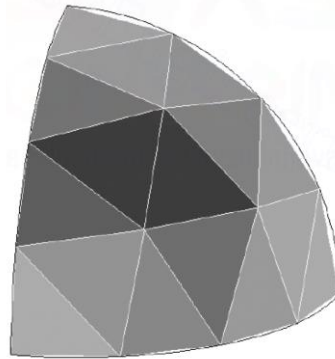
Figure 2.12 Hemispherical domain discretized into elements of simple geometry [39]

A common algorithm for finding the solution of simulation software is Newton's method. Newton's method, also known as the Newton-Raphson method, is an algorithm for finding roots of the equation. This algorithm starts with an initial guess which is reasonably close to the true root, then approximates the function by its tangent line using calculus [40]. As shown in Figure 2.13, let f(x) be a well-behaved function and let x_s be a root of the equation f(x)=0. In the beginning, starting with an estimate x_0 as the initial guess and drawing the tangent line at x= x_0. The new estimate x_{NR} is obtained by sliding from the point of (x_0, f(x_0)) to the x-intercept of the tangent line. After that repeating this step until the x_{NR} is closed to the real root of the equation (x_s) [41]. The equation for finding x_{NR} estimate is following in Eq. 2.27.

$$x_{NR} = x_0 - \frac{f(x_0)}{f'(x_0)}$$

(Eq. 2.27)
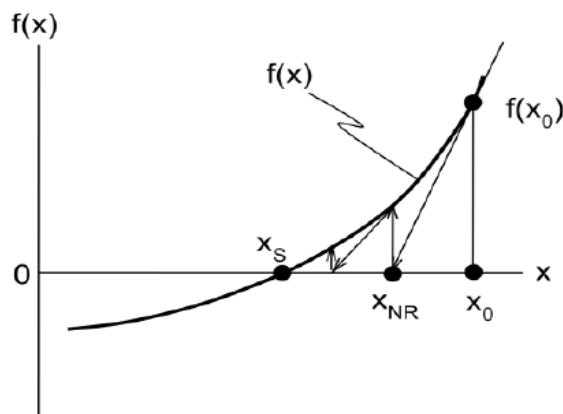
Figure 2.13 The algorithm of Newton's method [41]

2.7 Literature review of previous model results

In order to study the effect of the different structures of catalyst in the packed bed reactor, the simulation studies have been applied to create the model for describing the phenomenon inside the reactor. The literature of previous model results is separated into two parts of the conventional pellet catalyst and the novel foam catalyst.

2.7.1 Conventional pellet catalyst

Joel M.Silva et al. (2016) [9] revealed the investigation of a phenomenological model for finding the suitable operating condition in the packed bed reactor of the GSR process. The parametric analysis considered the difference of temperature: 748-848 K, water to glycerol feed ratios: 3-12, and pressure: 1-5 atm. The simulation study used MATLAB software for solving the result of different operating conditions. The catalyst in the reactor was assumed as a powder spherical catalyst with a catalyst particle diameter of 1.40×10^{-4} m and neglected any transportation within the catalyst. Moreover, this study used the power-law kinetic model of glycerol decomposition reaction to present the reaction mechanism in the modeling. The study result presented the maximum amount of 4.93 mol of H2 per mol of glycerol fed. This value was observed at a temperature of 848 K, WGFR of 9, and pressure of 2 atm, as shown in Figure 2.14.
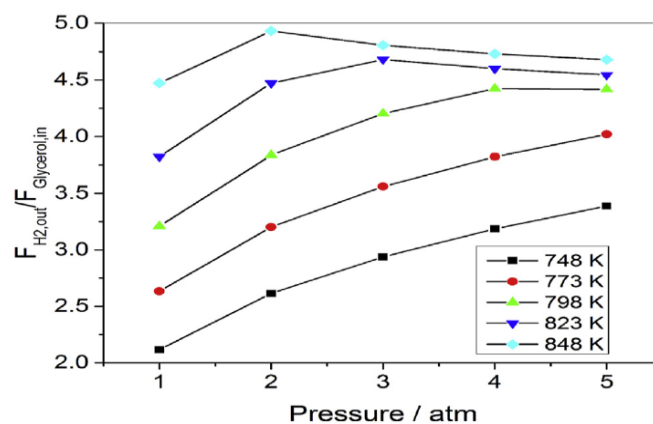
Figure 2.14 Effect of pressure on the amount of hydrogen produced per glycerol fed to the reactor at different temperature and WGFR of 9 [9]

Diego Rua and Liliana Hernandez (2016) [42] revealed the phenomenological evaluation of industrial reformers for the GSR process by studying the effect of catalyst particle size and shape under an adiabatic condition in a 1D heterogeneous model. The operation was set the mass fraction of glycerol in feed at 0.35, temperature and pressure of feed at $500^{\circ}C$ and 10 bar and the mass flow of feed at 3.2 (kg/m^2•s) for all case. The reactor behavior was evaluated for spheres and raschig rings with particle diameters of 8.5 mm, 17 mm, and 25.5 mm in a reactor length of 10 m. The kinetic model in this study used only the power-law type of the glycerol decomposition reaction to represent the GSR behavior. The results of this study showed the effect of catalyst structure on the glycerol conversion and pressure change, as shown in Figure 2.15 a.). For both catalyst shapes, the larger particle (25.5 mm) required a longer reactor for reaching 100% glycerol conversion, as compared with the reactor filled with the smallest particle (8.5mm). The small particle can reach the complete conversion by using the short reactor length but its dense particles reducts the void fraction and increas the pressure drop in the packed bed reactor, as shown in Figure 2.15 b.).
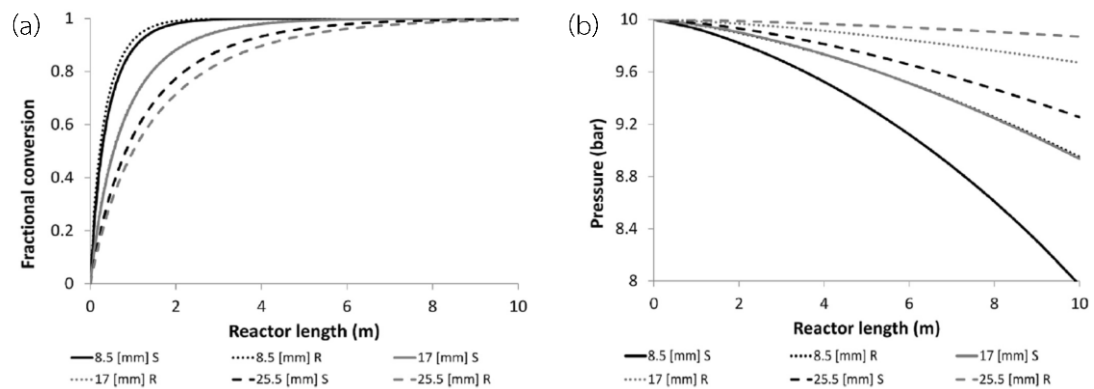
Figure 2.15 Comparative results between different catalyst size and shape [42]

John Eamon Kent (2013) [43] revealed the simulation of the GSR process in an industrial-sized packed bed reactor to understand its transport limitations. This study considered the effect of internal diffusion limitations and effectiveness factors in the reactor by comparing different spherical catalyst diameters (1-1/64 inches). From the

study results, the limiting step of the GSR process was an internal diffusion limitation because most of the glycerol consumed only on the edge of the catalyst particle, as shown in Figure 2.16. The diffusion-limited can improve by using the smaller catalyst particles, but the small particles will increase the pressure drop in the reactor.
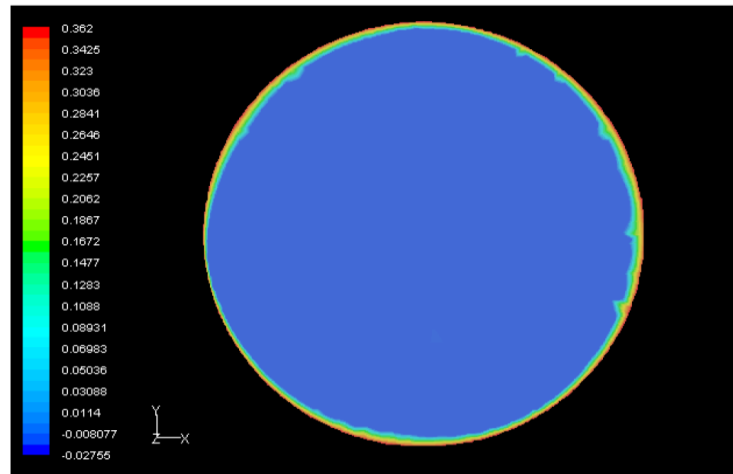
Figure 2.16 1-inch diameter catalyst cross-section of glycerol mass fraction [43]

From previous studies of conventional catalysts, the GSR process is performed as the diffusion-limited behavior while the external surface area of the catalyst is performed as a reaction area. The limitation of the catalyst size became a serious problem because the large catalyst size provided the large transport resistances while the small catalyst size provided the large pressure drop that affected the pump working.

2.7.2 Foam catalyst

Gregor D et al. (2019) [17] revealed the modeling packed bed reactor from open-cell metal foams as a catalyst structure. A pseudo-homogeneous model is applied to describe pressure drop and heat transfer inside the foam pellets. The open-cell solid foams are characterized by a high porosity that increased the surface area of catalyst in the reaction, as shown in Figure 2.17.
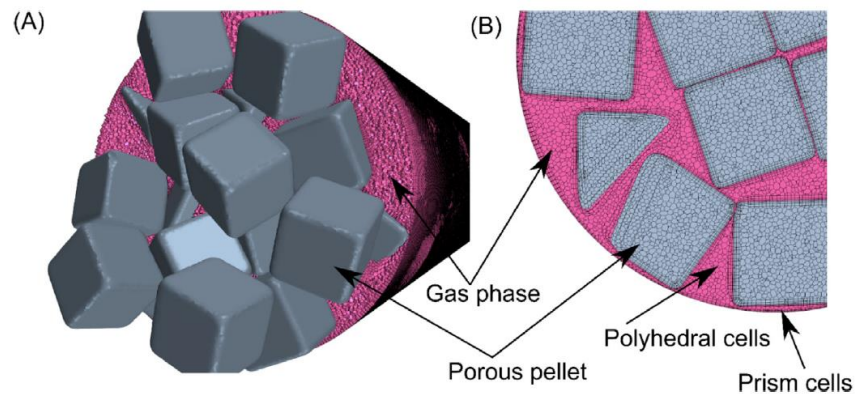
Figure 2.17 Characteristics of open cell solid foam

(A) Metal foams of different size and shape.

(B) Detail with cell size definition (here, nominal cell size is 3 mm) [44]

From the study results, the open-cell foam catalyst showed excellent radial heat transfer characteristics. Moreover, this study has been compared the result of pressure drop between two different catalyst structures because this parameter affected to the operating cost in the reactor. For the bed of solid pellets, the pressure drop was 1141 Pa, where the pressure drop of a porous cube (open-cell foams) was only 560 Pa. From the result, the porous foam catalysts improved the performance of heat transfer, pressure drop, and mixing behavior in the packed bed reactor.

V. Palma et al. (2018) [45] revealed the study of structured catalysts in the water gas shift reaction by using CFD modeling to investigate two different catalytic configurations between the powder catalysts and the novel foam catalysts. The different types of material properties were simulated and shown in Table 2.5.

Table 2.5 Material properties of powder catalyst and foam catalyst [45]

Material property	Powder catalysts	Foam catalysts
Thermal conductivity	1.4 $Wm^{-1}K^{-1}$	218 $Wm^{-1}K^{-1}$
Porosity	0.4	0.93
Permeability	10^{-5} m^2	10^{-6} m^2

A model of the adiabatic reactor was set for both powder catalysts and foam catalysts. It demonstrated that the use of highly conductive carriers reduced the temperature difference in the reactor. The use of a highly active catalytic formulation coupled with the conductive carrier provided the possibility to realize a strong intensification of the water gas shift process. Moreover, the studies of CO molar fraction in both catalyst structures have been investigated to show the CO mass balance along the reactor length, as shown in Figure 2.18. The CO molar concentration showed in the range of 6.22×10^{-4} to 0.08 mol/m^3 and 9.97×10^{-7} to 1.43×10^{-4} mol/m^3 for powder catalyst and foam catalyst, respectively. The result showed the effect of the high porosity of the foam catalyst that facilitated the mass transfer and increased the reaction within the reactor.
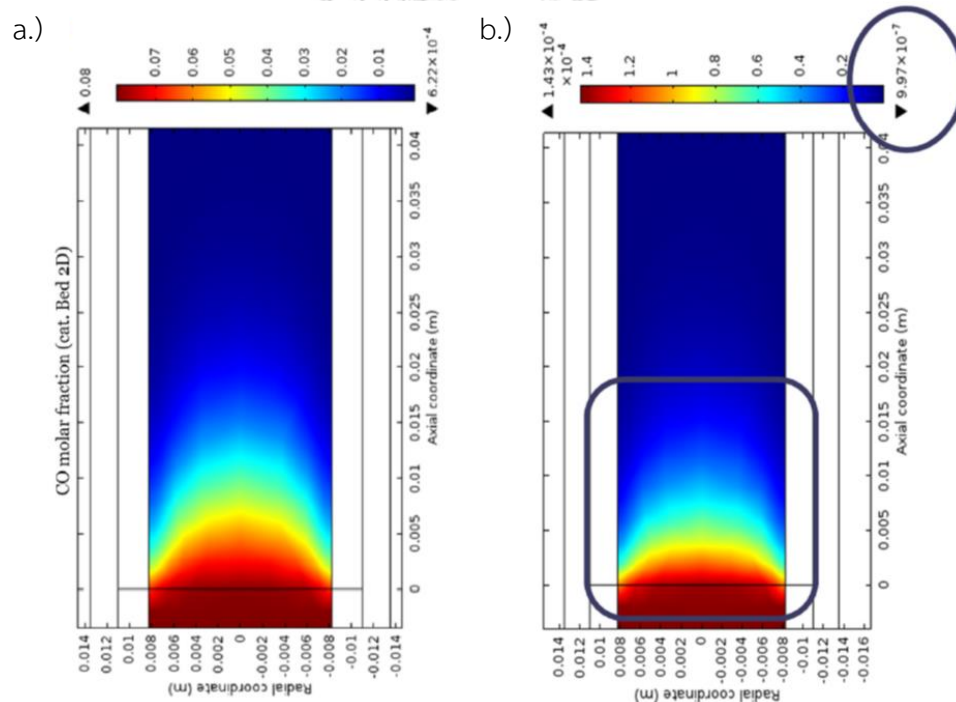
Figure 2.18 2D simulation of the CO molar concentration (mol m^{-3})
a.) powder catalyst, and b.) foam catalyst [45]

G. Anna et al. (2019) [44] revealed the comparison between solid foam, a packed bed of 3 mm grains, and 100 cpsi monolith to study the modeling results of the selective catalytic reduction of nitrogen oxides (SCR deNOx) process. The

characteristic parameters of different catalyst are shown in Table 2.6. Moreover, the reaction conversion of this study was calculated based on temperature and superficial velocity constant.

Table 2.6 The characteristic parameters of the different catalyst [44]

	NC 0610 foam	NC 2733 foam	monolith	grain
S_v (m^2/m^3)	1298	3616	1339	1240
d_h (m)	2.73×10^{-3}	9.61×10^{-3}	2.15×10^{-3}	1.23×10^{-3}

The study results showed in Figure 2.19. NC 2733 foam performed the higher reaction conversion and used a shorter reactor length to achieve 100% conversion. On the other hand, another catalyst (NC 0610 foam, monolith, and packed bed grain) achieved 100% conversion at the longer reactor length. This result was caused by a specific surface area of the NC 2733 foam much larger than the other catalyst about three times. The large specific surface area significantly increased the reaction rate in the reactor.
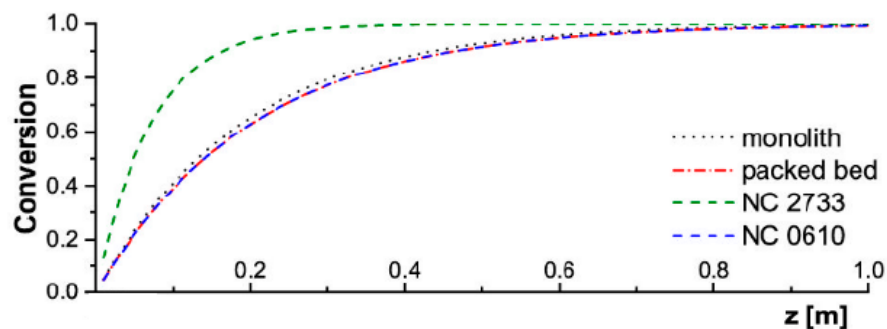
Figure 2.19 Conversion profile along the reactor length of different catalyst for SCR deNOx process in T=723K and u=2m/s [44]

The previous studies performed the advantage of foam catalysts over the classic packed bed particles in a part of the momentum, heat, and mass transfer under the same condition of various reactions. Most studies only compared between the

foam catalyst and the small catalyst size in the laboratory reactor scale instead of the industrial scale with real catalyst size.

The previous simulation studies of the GSR process used the power-law type of the overall reaction or only glycerol decomposition reaction to study the reaction phenomena inside the reactor. Moreover, in part of the catalyst structures, the previous studies commonly used the pellet or powder catalyst in the packed bed reactor and did not study other novel catalyst structures. From all the problems mentioned above, the comparison of the novel foam catalyst and the conventional pellet catalyst of the GSR process in the industrial scale with the separating kinetic model of the glycerol decomposition, water gas shift, and CO-methanation reaction became an interesting subject to investigate in this research.
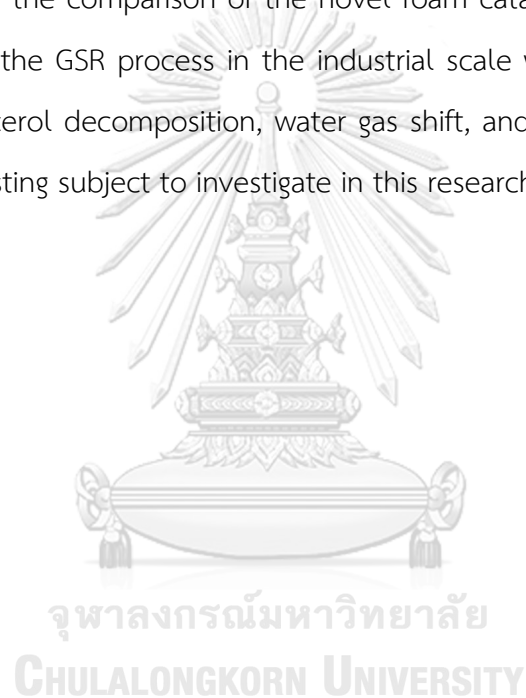
CHAPTER 3 SIMULATION AND DESIGN

This chapter explains the method for simulation and design of the packed bed reactor with different catalyst structures (conventional pellet catalyst and novel foam catalyst) for hydrogen production of glycerol steam reforming (GSR) process. The solving of numerical solution achieved by COMSOL Multiphysics version 5.3a with finite element method. The method represented all of the momentum, heat, and mass transfer phenomena inside the packed bed reactor.

3.1 Model description
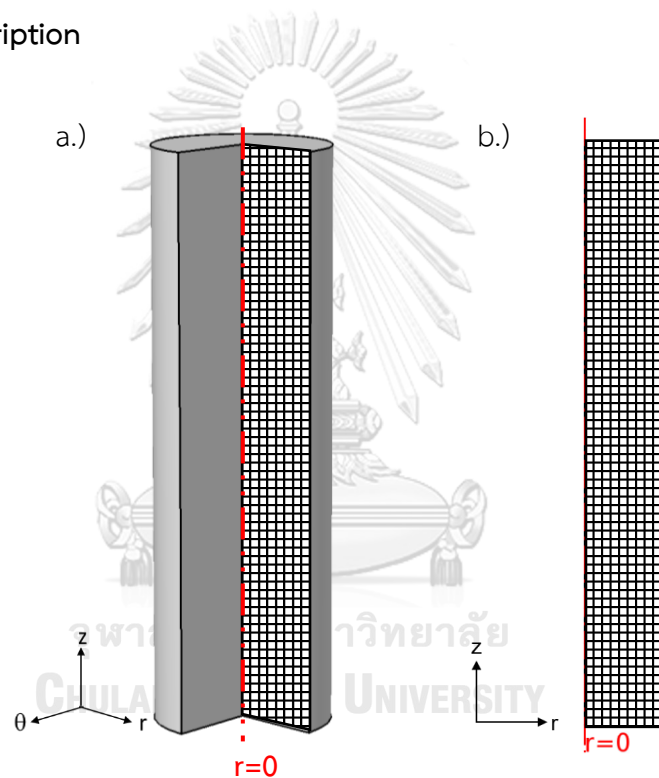
Figure 3.1 The schematic of the packed bed reactor

a.) 3D geometry, b.) 2D geometry

Generally, the packed bed reactor is a cylindrical shape, as presented with a 3D geometry in Figure 3.1 a). Because of the very complex calculation of the 3D geometry, an assumption of uniformly distributed catalysts has been applied in the geometry to provide symmetric cylindrical characteristics. As a result, a 3D geometric cylindrical coordinate (r, θ, z) is reduced to be a 2D geometric cylindrical coordinate

(r, z) by neglecting any change in an angular direction, as shown in Figure 3.1 b.). In the study, an industrial-scale reactor with 2D-symmetric cylindrical coordinates is used to simulate the GSR process with length and diameter of 15 m and 0.15 m, respectively. In the reactor, a mixture of glycerol and steam flows through the Ni/Al_2O_3 catalysts and the reaction will take place around the catalyst domains. According to the significant effect of the catalyst domains on the reactor design, the different structures of catalyst domains are one of the interesting parameters to improve the reaction performance. From the above reason, the study is divided the catalyst structure into two cases consisting of the conventional pellet catalysts and the novel foam catalyst to study and compare the reactor performances of the GSR process.

In the simulation, the operating parameters are expressed in Table. 3.1 where the reactor with the conventional pellet catalyst and the novel foam catalyst are simulated under the same operating condition in order to compare the effect of the catalyst structure on the glycerol conversion, temperature distribution, pressure distribution, hydrogen yield, and components distribution of the GSR process along the reactor length.

Table 3.1 The operating parameters for packed bed reactor

Parameter	Value
Inlet pressure (Pa)	2.02×10^5
Inlet temperature (K)	823
Steam to glycerol feed ratio (mole basis)	9:1
Linear inlet velocity (m/s)	5

3.2 Model assumptions and equations

3.2.1 Model assumptions

The fluid dynamic simulation was performed on the system with the different catalyst structures, in order to study the macroscopic flow regime, heat transfer, and

reaction inside the reactor. The phenomenological model of the work followed with the below assumption:

- A pseudo-homogeneous model is used in the study to describe momentum, heat, mass, and chemical reaction in the packed bed reactor.

- The catalyst domains are assumed to be homogeneous, in which the catalysts uniformly distribute along the reactor length with constant open porosity.

- The model is performed for the 2D-symmetric cylindrical coordinates (r, z) by neglecting angular direction. As show in Figure 3.1, the packed bed reactor is presented as symmetric rectangular geometry.

- The model is calculated under the steady state condition by neglecting any parameter change with time.

- The mixture reactants were fed at high temperature (823K) and low pressure (2.02×10^5 Pa). Under these conditions, the mixture reactants are presented an ideal gas behavior.

- Thermo-physical properties such as diffusivity, conductivity, and heat capacity of the mixture reactants are assumed constant because the mixture reactants were fed to the reactor in dilute form (WGFR is 9:1 base on mole basis).

- The model was performed in the industrial scale with high flowrate and dominated by convection transport, then an axial dispersion was neglected.

- The model is simulated under the non-isothermal constant-wall temperature conditions (wall and inlet of the reactor maintain at 823K).

3.2.2 Governing equations

From the general form of the governing equations in Chapter 2, the 2D-symmetric cylindrical coordinates and model assumptions have been applied to the governing equations (Eq. 2.17-2.21). The equations of mass, energy, and momentum balance of the simulation were presented in (Eq. 3.1–3.3).

- **The mass balance**

$$u\frac{\partial C_i}{\partial z} = -\frac{\partial J_i}{\partial r} - \frac{1}{r}J_i + S_v\sum_{j=1}^{n}\upsilon_{ij}R_j \qquad \text{(Eq. 3.1)}$$

- **The energy balance**

$$\rho_f C_{P,f} u\frac{\partial T}{\partial z} = -\frac{\partial q}{\partial r} - \frac{1}{r}q + S_v\sum_{j=1}^{n}(-\Delta H_j)R_j \qquad \text{(Eq. 3.2)}$$

- **The momentum balance**

In the simulation, Forchheimer equation is used to calculate the pressure distribution in form of a pseudo-steady state momentum balance where the pressure drop in the reactor is dominated by the catalyst structure inside the reactor. In Eq. 3.3, the Forchheimer equation shows the summation between two terms of laminar and turbulent regimes. The first term of the laminar flow condition shows the viscous effect, while the second term of the turbulent flow condition shows the inertial effect in the porous media.

$$\frac{\partial P}{\partial z} = -\frac{\mu_f}{K}u(r) - \frac{\rho_f}{C_F}u^2(r) \qquad \text{(Eq. 3.3)}$$

where the permeability (K) and Forchheimer-coefficient (C_F) of the spherical pellet catalyst and foam catalyst can be calculated using (Eq. 3.4 – 3.5) and (Eq. 3.6 – 3.7), respectively.

The spherical pellet catalyst [46]:

$$K = \frac{\varepsilon_o^3 d_P^2}{150(1-\varepsilon_0)^2} \qquad \text{(Eq. 3.4)} \qquad\qquad C_F = \frac{\varepsilon_o^3 d_p}{1.75(1-\varepsilon_o)} \qquad \text{(Eq. 3.5)}$$

In spherical pellet catalyst, the characteristic length of the conventional pellet catalyst is a spherical particle diameter (d_p).

The foam catalyst [47]:

$$K = \frac{\varepsilon_o d_h^2}{32\tau^2} \qquad \text{(Eq. 3.6)} \qquad\qquad C_F = \frac{\varepsilon_o^2 d_h}{2\tau^3} \qquad \text{(Eq. 3.7)}$$

In foam catalyst, the characteristic length of the novel foam catalyst is a hydraulic diameter (d_h) by respecting the foam structure with the spherical pellet catalyst.

- **Catalyst geometrical characterization**

In the simulation, both catalyst structures used different correlations to represent their characteristics, where the correlations are expressed in Table 3.2.

Table 3.2 The correlations of the catalyst structures [47]
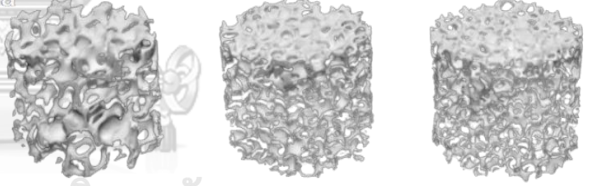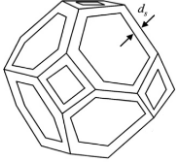
Parameter	Pellet catalysts	Foam catalyst		
		10PPI	20PPI	30PPI
geometry	(spherical shape)	(foam structure cut to be a cylindrical shape)		
ε_o		$\varepsilon_o = 1 - \left(\dfrac{\rho_{bed}}{\rho_{cat}} \right)$		
Characteristic length	measured (d_p)	$d_h = \dfrac{4\varepsilon_o}{S_v}$		
d_{por}	measured			
S_v	$S_{v,pellet} = \dfrac{6}{d_p}\left(1-\varepsilon_o\right)$	$S_{v,foam} = \dfrac{3}{d_s}\left(1-\varepsilon_o\right)$		

Table 3.3 (continue) The correlations of the catalyst structures [47]

Parameter	Pellet catalysts	Foam catalyst		
		10PPI	20PPI	30PPI
d_s	-	$d_s = \dfrac{0.5338 d_{por} \sqrt{(1-\varepsilon_o)}}{1 - 0.971\sqrt{(1-\varepsilon_o)}}$		
τ	measured	$\tau = 1 + \dfrac{d_{por}}{d_h}$		

The different characteristics are presented in the parameters of open porosity (ε_o), characteristic length, pore diameter (d_{por}), and the specific (volumetric) surface area (S_v), as shown in Table 3.3.

Table 3.4 The different dimension of catalyst structures [32, 48]

Parameters	Pellet catalysts	Foam catalyst		
		10PPI	20PPI	30PPI
d_p (m)	2.54×10^{-2}	-	-	-
d_{por} (m)	1.40×10^{-8}	1.52×10^{-3}	9.40×10^{-4}	7.50×10^{-4}
d_s (m)	-	4.51×10^{-4}	3.11×10^{-4}	2.75×10^{-4}
d_h (m)	-	4.02×10^{-3}	2.35×10^{-3}	1.79×10^{-3}
ε_o	0.4	0.87	0.85	0.83
S_v (m^2/m^3)	1.41×10^{2}	8.65×10^{2}	1.44×10^{3}	1.85×10^{3}
τ	3.54	1.38	1.40	1.42

- **Kinetic model**

The reactions of the GSR process in this study considered three main equilibrium reactions (glycerol decomposition, water-gas shift, and CO-methanation), as shown in Eq. 2.2-2.4, and neglected coke formation reaction due to high steam and glycerol feed ratio [28].

- Glycerol decomposition

$$C_3H_8O_3 \longrightarrow 3CO + 4H_2 \qquad (\Delta H_r^0 = +251 \text{ kJ/mol}) \qquad \text{(Eq. 2.2)}$$

- Water-gas shift

$$CO + H_2O \rightleftharpoons H_2 + CO_2 \qquad (\Delta H_r^0 = -41 \text{ kJ/mol}) \qquad \text{(Eq. 2.3)}$$

- CO-Methanation

$$CO + 3H_2 \rightleftharpoons CH_4 + H_2O \qquad (\Delta H_r^0 = -206 \text{ kJ/mol}) \qquad \text{(Eq. 2.4)}$$

In this study, the kinetic model of glycerol steam reforming reaction over Ni/Al$_2$O$_3$ catalyst was applied to the simulation because of the extensive studies of the kinetic modeling in three main equilibrium reactions of the GSR process. The kinetic rate of the glycerol decomposition reaction [35] is shown in Eq. 3.8, and the water-gas shift and CO-methanation reaction [26] are shown in Eq. 3.9 – 3.10, whereas other parameters is shown in Table 3.4.

Glycerol decomposition (1st reaction):

$$R_1 = k_1 p_{C_3H_8O_3}^{\beta} \qquad \text{(Eq. 3.8)}$$

Water-gas shift (2nd reaction):

$$R_2 = \frac{k_2}{p_{H_2}}\left(p_{CO}p_{H_2O} - \frac{p_{H_2}p_{CO_2}}{K_2} \right)\left(\frac{1}{\Omega^2} \right) \qquad \text{(Eq. 3.9)}$$

CO methanation (3rd reaction):

$$R_3 = \frac{k_3}{p_{H_2}^{2.5}}\left(\frac{p_{H_2}^2 p_{CO}}{K_3} - p_{CH_4}p_{H_2O} \right)\left(\frac{1}{\Omega^2} \right) \qquad \text{(Eq. 3.10)}$$

The auxiliary equations of the kinetic model were presented in Eq. 3.11–3.15.

$$k_j = k_{0,j} \exp\left(\frac{-Ea_j}{RT} \right) \qquad \text{(Eq. 3.11)}$$

$$K_2 = \exp\left(\frac{4400}{T} - 4.036\right) \qquad \text{(Eq. 3.12)}$$

$$K_3 = \exp\left(-\frac{26830}{T} + 30.114\right) \qquad \text{(Eq. 3.13)}$$

$$\Omega = 1 + K_{CO}p_{CO} + K_{H_2}p_{H_2} + K_{CH_4}p_{CH_4} + K_{H_2O}\frac{p_{H_2O}}{p_{H_2}} \quad \text{(Eq. 3.14)}$$

$$K_i = K_{0,i}\exp\left(\frac{-\Delta H_i}{RT}\right) \qquad \text{(Eq. 3.15)}$$

3.3 COMSOL Multiphysics

3.3.1 Module configuration

In this study, the module configurations comprise:

- Transport of diluted species in porous media module is used to describe mass transfers of fluid in reactor and catalysts according to the mass balance in Eq. 3.1,

- Heat transfer in porous media module is used to describe heat transfers of fluid in reactor according to the energy balance in Eq. 3.2,

- Chemistry module is used to describe the kinetic equations of GSR reactions that occurred on the catalyst surface, and

- The Forchheimer equation is applied in Coefficient form PDEs node to describe the pressure change in the reactor according to the momentum balance in Eq. 3.3.

All four physic modules have been applied to the COMSOL Multiphysics program to describe all phenomena that occurred in the reactor model.

Table 3.5 Kinetic parameters for the different reactions [26, 35]

Parameter		Value
Order of reaction	β	1.2
Activation energy	E_1 (kJmol^{-1})	35.80
	E_2 (kJmol^{-1})	67.13
	E_3 (kJmol^{-1})	240.10
Pre-exponential factor of reaction j	$k_{0,1}$ (molkPa$^{-\beta}$m^{-2}s^{-1})	3.48×10^{-3}
	$k_{0,2}$ (molkPa^{-1}m^{-2}s^{-1})	5.84×10^{-1}
	$k_{0,3}$ (molkPa$^{0.5}$m^{-2}s^{-1})	1.26×10^{12}
Adsorption constant of species I at reference temperature of 823K	$K_{0,CO}$ (kPa^{-1})	8.23×10^{-7}
	$K_{0,H2}$ (kPa^{-1})	6.12×10^{-11}
	$K_{0,CH4}$ (kPa^{-1})	6.65×10^{-6}
	$K_{0,H2O}$ (-)	1.77×10^{3}
Heat of adsorption of species i	ΔH_{CO} (kJmol^{-1})	-70.65
	ΔH_{H2} (kJmol^{-1})	-82.90
	ΔH_{CH4} (kJmol^{-1})	-38.28
	ΔH_{H2O} (kJmol^{-1})	88.68

3.3.2 Boundary condition

In the mathematical equations, boundary conditions are necessary constraints to solve the problems in the reactor model. As shown in Table 3.5, the feed parameters of temperature, pressure, and reactant concentration were set to the boundary condition. All parameters are set to be constant at the reactor inlet. At the reactor wall, the temperature is also set to be constant with the feed temperature to maintain the adiabatic condition, and the gradient of any components set to be zero.

Table 3.6 The boundary conditions

Location	Mass balance (eq. 3.1)	Energy balance (eq. 3.2)	Momentum balance (eq. 3.3)
Reactor inlet $z = 0$	$C_i(0,r) = C_i^{in}$	$T(0,r) = T^{in}$	$P(0,r) = P^{in}$ $u(0,r) = u^{in}$
Reactor outlet $z = L_{re}$	$J_i(L_{re},r) = 0$	$q_i(L_{re},r) = 0$	-
Reactor wall $r = R_{re}$	$J_i(0, R_{re}) = 0$	$T(0, R_{re}) = T^{wall} = T^{in}$	$u(z,R_{re}) = 0$

The global parameters and variables were added to explain the operating condition, fluid and catalyst properties, mass transfer correlation, and diffusion coefficients in the COMSOL Multiphysics program. After the module configurations and the boundary condition added to this program, a finite element method (FEM) will solve the problems. Under the FEM, the model is separated into several elements and set the simultaneous algebraic equations to solve with a finite number of degrees of freedom.

3.3.3 Mesh geometry

In the simulation, mesh quality has influenced to the accuracy, and speed of the simulation. The high quantity of mesh provides more accuracy but also takes more time to calculate. To avoid unnecessary mesh quantity, mesh analysis must be studied in the simulation. As shown in Figure 3.2, a mapped structure with a rectangular shape is created on the geometry. The average quality of the mapped structure equaled 1.0, which meant this structure suitable for geometry. The mesh analysis has been performed for mapped meshes of 504, 1053, 2985, 4320, 5670, 6244, 7680, 8488, 9855, 10800, and 12600 domain elements. As shown in Figure 3.3, the simulation results of the glycerol conversion were almost constant after 7680 domain elements. Therefore, this point is used as mesh geometry for the study.
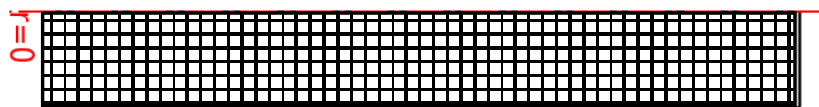
Figure 3.2 The mapped mesh
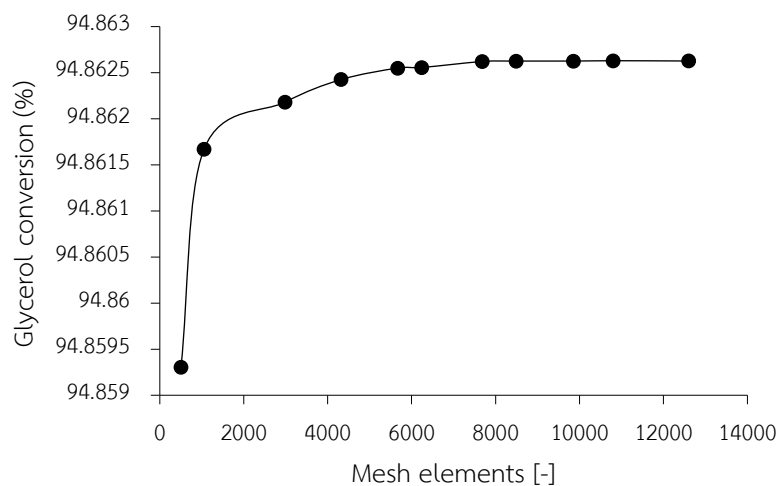
Figure 3.3 Mesh analysis

3.4 Methodology

The methodology of the study is presented in Figure 3.4. First of all, the simulation model must be checked the validation and verification via the results from previous studied. Then the mesh analysis has been studied to check the accuracy of the model, and the comparison between different catalyst structures will simulate via the following three steps:

Step 1: Validating and verifying the model study of the conventional pellet catalyst with the previous study of the GSR process to ensure the accuracy of the simulation results.

Step 2: Creating the model study of the novel foam catalyst in the GSR process by dividing the foam catalyst into 3 cases of 10, 20, and 30 PPI.

Step 3: Comparing the simulation results between both catalyst structures of the conventional pellet catalyst and the novel 10-30 PPI foam catalyst.

Wherein the simulation results are shown in Chapter 4 in terms of the glycerol conversion, temperature distribution, pressure distribution, hydrogen yield, and components distribution of the GSR process along the reactor length.
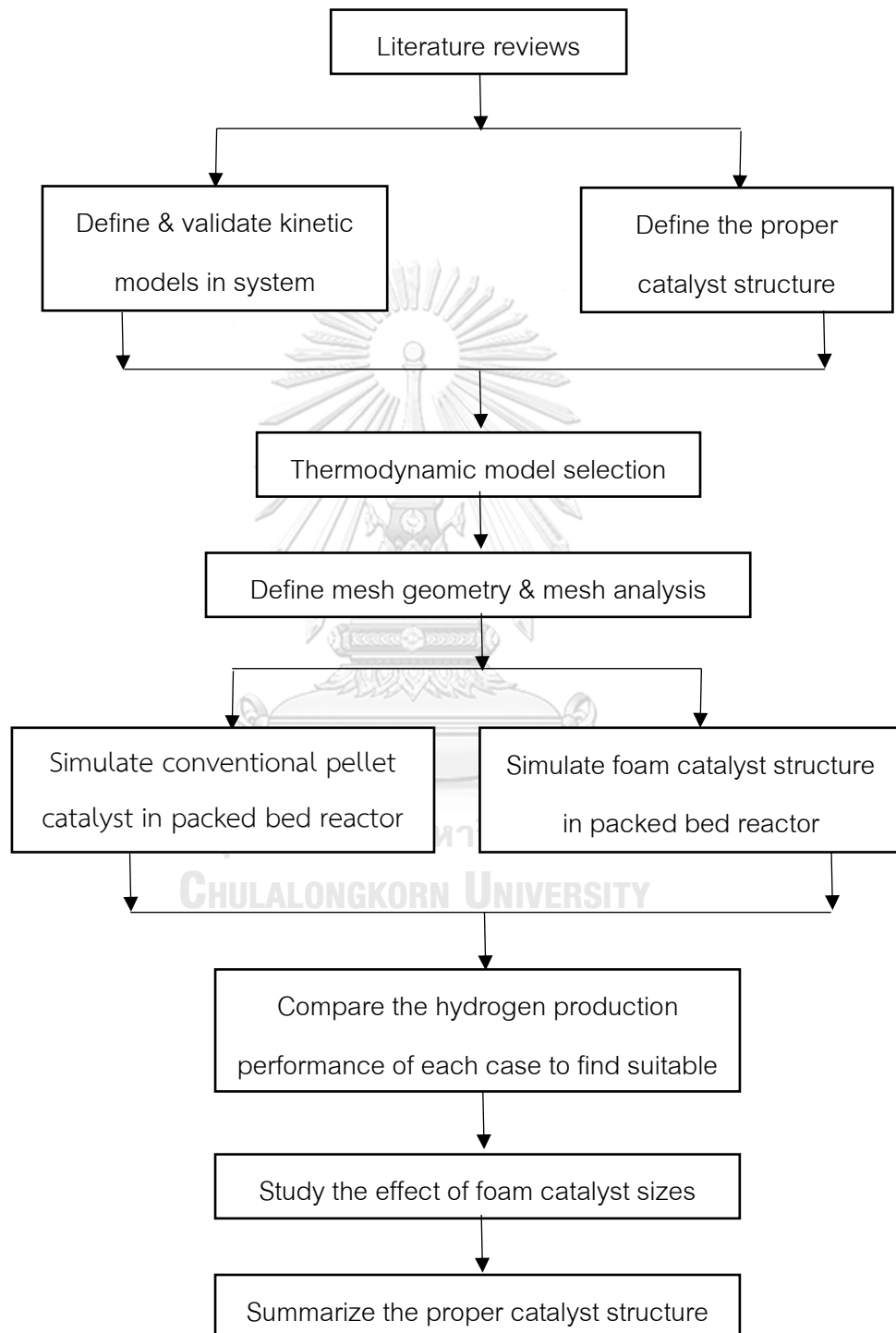
Figure 3.4 Methodology

CHAPTER 4 RESULTS AND DISCUSSION

This chapter shows the comparative simulation results between the conventional pellet catalyst and the novel foam catalyst of the GSR process. The results and discussion include 4 main parts; 1.) The model validation & verification, 2.) The comparison of catalyst characteristics, 3.) The comparison of process performances between the conventional pellet catalyst and the novel foam catalyst, and 4.) The optimal design.

4.1. The model validation & verification

The model was verified and validated to ensure the correctness of its output results in terms of glycerol conversion. The simulation study of Macdonald, Bryan et al., (2014) [48] is used as the reference results for comparison. The characteristics of the reactor and the operating conditions for reference results are concluded in Tables A1 and A2 in Appendix A. The reference results were simulated for an industrial-scale packed bed reactor with GSR process under adiabatic condition.

4.1.1 Model verification

The mass balance between the reactor inlet and outlet is calculated to verify the model accuracy, wherein the boundary is created around the reactor unit, as shown in Figure 4.1. The reactants are fed only glycerol and water at the inlet, while the output contained glycerol, water, hydrogen, carbon dioxide, carbon monoxide, and methane. The results are shown in Table 4.1 in terms of the component mass flow rates. The results displayed a slight difference between the values of the inlet and the outlet where the deviation was within 1×10^{-3} kg/hr.
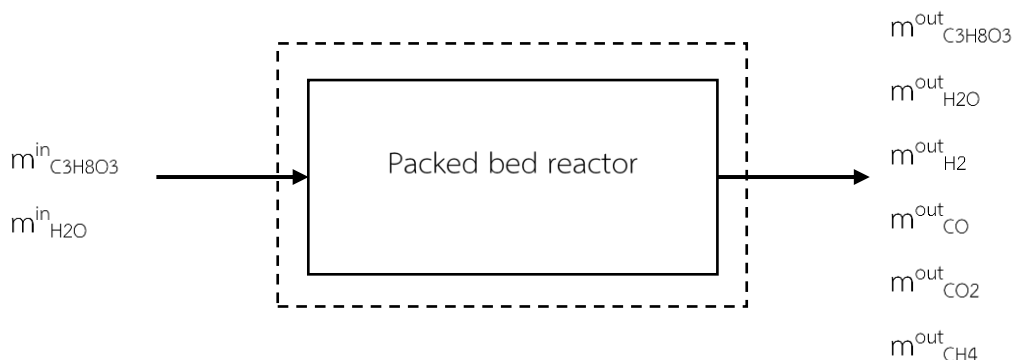
Figure 4.1 Boundary for mass balance calculation

Table 4.1 The mass flow (kg/hr) at inlet and outlet of the reactor

Mass flow (kg/hr)	Inlet	Outlet
$C_3H_8O_3$	23.857	5.299
H_2O	214.708	135.149
H_2	-	61.352
CO	-	3.417
CO_2	-	28.090
CH_4	-	5.256
Total	238.565	238.564

Moreover, the temperature and pressure distributions along the reactor length are also investigated in order to assess the reactor behaviors. The temperature distribution along 4 m length is showed in Figure 4.2. At the first 3 m length, the temperature distribution dissipates from 823 to 760 K because of the endothermic behavior of the glycerol decomposition reaction. Then the temperature will increase along the reactor length because the products of hydrogen and carbon monoxide are reacted with the feed water and the reaction has been shifted toward the water-gas shift and the CO-methanation reactions that are exothermic.
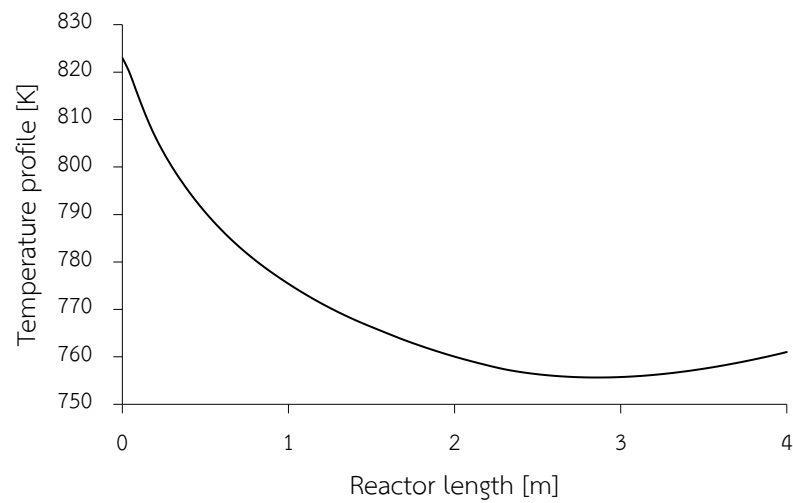
Figure 4.2 Temperature distribution along 4 m length

Similarly, the pressure distribution along 4 m length is shown in Figure 4.3. The pressure distribution gradually drops from 202 to 175 kPa because of the friction force from the catalyst domains inside the reactor.
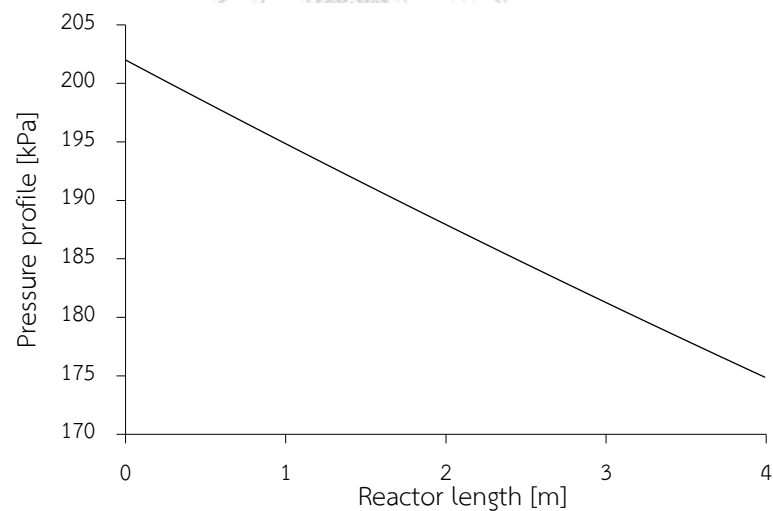
Figure 4.3 Pressure distribution along 4 m length

4.1.2 Model validation

The result in Figure 4.4, line graph represents the results from the model prediction and red point represents the data from reference results [48], showed a good agreement between the model prediction and the reference results [48] by

concerning the glycerol conversion along the reactor length. The relative error in term of mean absolute percentage error (MAPE) between the model prediction and the reference result [48] is also calculated, the average error and the maximum error are 1.71% and 2.55%, respectively.
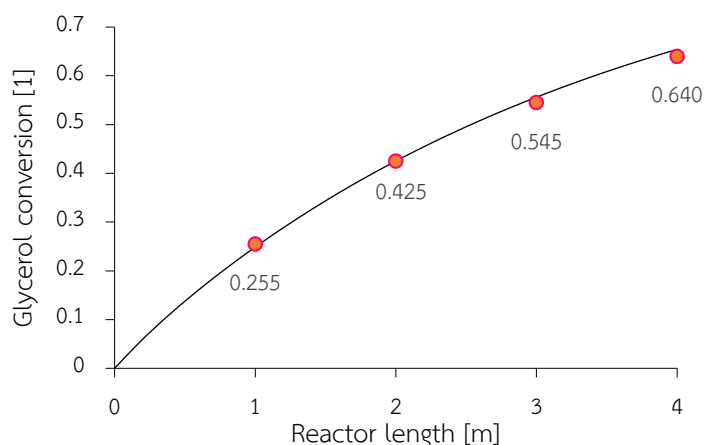
Figure 4.4 The glycerol conversion along the bed length comparing between this study and Macdonald, Bryan et al., (2014) [48]

4.2. The comparison of catalyst characteristics

Each catalyst structure provides different characteristics in terms of geometry, porosity, specific surface area, and effective diffusivity. All parameters influence on the reactor and reaction performances. The parameters of open porosity, total catalyst weight, and total catalyst external surface area are shown in Table 4.2, whereas the values of the diffusivity are explained in Table B1 and B2 in Appendix B.

Table 4.2 The catalyst characteristics

	1-inch pellet	10PPI	20PPI	30PPI
Open porosity	0.4	0.87	0.85	0.83
Total catalyst weight (kg)	307.59	119.81	138.24	156.67
Total catalyst external surface area (m^2)	37.32	229.35	382.96	491.09

The open-cell structure of foam catalyst not only increases the open porosity but also improves the total catalyst weight and catalyst external surface area inside the packed bed reactor. As presented in Table 4.2, all foam sizes presented the high value of open porosity and total catalyst external surface area and the low value of total catalyst weight compared to the 1-inch pellet. The higher open porosity increased the passage portion of fluid inside the reactor and lowered the pressure drop along the reactor length. Moreover, the lower catalyst weight of foam catalyst reduced the weight of reactor which is easier maintenances than a heavy reactor.

According to the diffusion-limited of the GSR reaction, the external catalyst surface area became a presenting parameter for the chemical reaction. In the comparison, all foam catalyst sizes provided the larger external surface area than the 1-inch pellet catalyst. This result is also affected from the natural open-cell structure of the foam catalyst that disclosed more than 80% of the catalyst surface.

4.3 The comparison of process performances between the conventional pellet catalyst and the novel foam catalyst

The different catalyst structures are compared between the conventional pellet catalyst (1-inch pellet spherical shape) and the novel foam catalyst (10PPI, 20PPI, and 30PPI) to study the GSR process performance in the packed bed reactor. The comparison of GSR process performances is divided into two parts of physical profile and chemical profile. Each catalyst structure is simulated under the same operating condition, as shown in Table 3.1. The physical profiles are compared in terms of pressure, velocity, and temperature, whereas the chemical profiles are compared in terms of glycerol conversion, hydrogen yield, and components distribution.

4.3.1 Physical profile
- **Pressure drop and velocity profile**

The graphical pressure drop and pressure contour along the reactor length are shown in Figure 4.5 and C1 of Appendix C, respectively. The reactor packed with the 1-inch pellet catalyst had a pressure drop of 85 kPa, while the reactor packed with the

10PPI, 20PPI, and 30PPI foam had a pressure drop of 4.83, 10.49, and 17.38 kPa, respectively. From the results, all foam catalyst sizes showed a lower pressure drop than the 1-inch pellet, for example, the 1-inch pellet gave five times of pressure drop more than the 30PPI foam catalyst case. Moreover, the 10PPI provided the lowest pressure drop.

The influenced parameter is explained from the open-cell structure of the foam catalyst. This structure increases the open porosity inside the reactor. The large open porosity increases the fluid flow passage and decreases the friction force from the catalyst domains inside the reactor. As explained in section 4.2, each foam catalyst provided about two times higher open porosity than the 1-inch pellet catalyst. The lower open porosity of the 1-inch pellet catalyst not only obstructs the fluid flow inside the reactor but also increases the pressure drop that influenced to the operating cost of the pump working in the system.
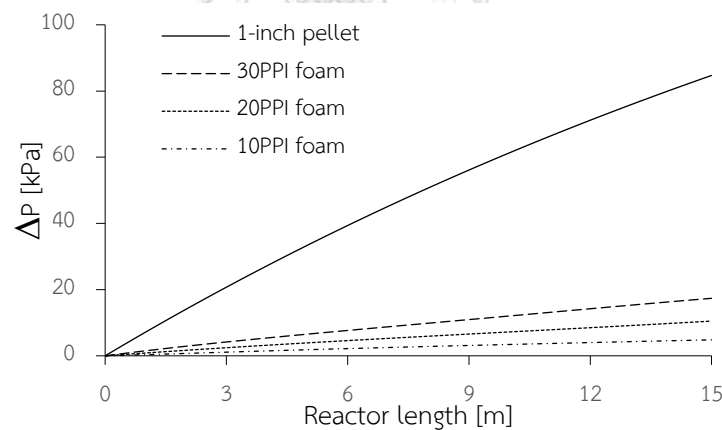
Figure 4.5 Pressure drop along the reactor length

Moreover, the velocity profile of the mixing fluid is also presented in Figure 4.6. In the 1-inch pellet case, the velocity almost directly increased along the reactor length and gave the outlet velocity at 12.50 m/s. Meanwhile in the 10PPI, 20PPI, and 30PPI foam case, the velocity drastically increased at the entrance length then the velocity slightly changed until the reactor end and gave the outlet velocity at 7.52, 7.75, and 8.04 m/s, respectively.

According to the Forchheimer equation, the velocity directly changed with the variation of pressure drop. But in the calculation, the velocity is transformed not only the pressure changes but also the variation of components inside the reactor, wherein the components change is presented in section 4.3.2. At the entrance length, the velocity change is dominated by the component variation because the reactants rapidly reacted and converted to more gas products. After the reactions slow down and the components change is almost constant, the pressure drop more influenced to the velocity change. Moreover, the low velocity profile of each foam case is also occurred from the large open porosity similarity to the explanation in the variation of pressure drop above.
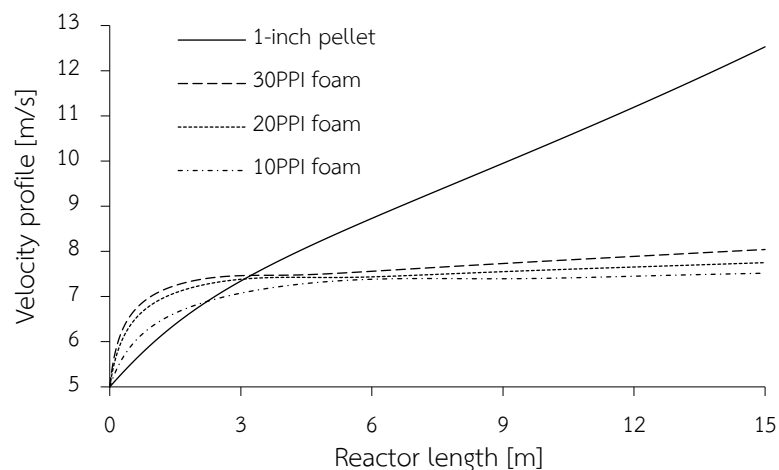
Figure 4.6 Velocity profile along the reactor length

Moreover, a velocity profile along the radial direction is also calculated to present the effect of open porosity and reactor wall. The velocity profile of each catalyst structure at the reactor center (7.5 m length) is shown in Fig. 4.7. At the reactor wall of all catalyst structures, the velocity profile is equal to zero due to the wall friction. Then the velocity gradually increases and constant along the cross-section position, wherein the maximum velocity is observed near the reactor wall because of the greater open porosity. At the position far from the reactor wall, the velocity profile

shows a uniform distribution due to the homogeneous porous medium assumption in the model generator.
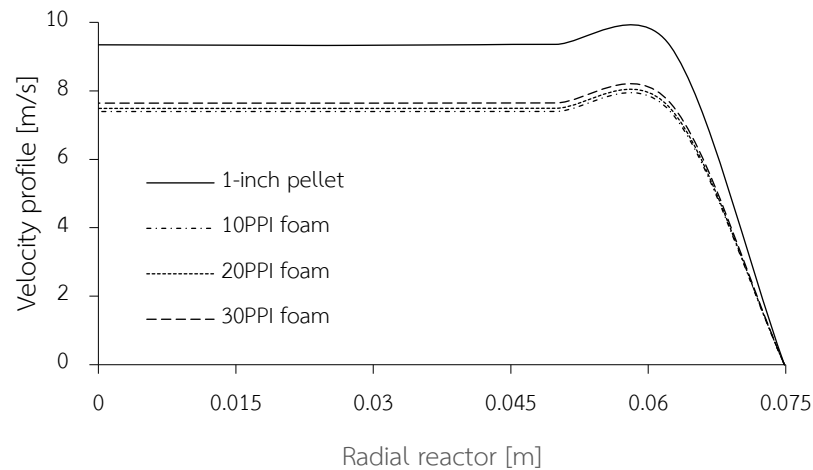
Figure 4.7 Velocity profile along the radial direction

- **Temperature profile**

The temperature contour at the first 3m length and 15m length are shown in Figure 4.8 and C2 of Appendix C, respectively, where the blue to red colour represented the low (700K) to high (820K) temperature region along the reactor length. In the radial direction of the reactor, all catalyst structures are performed the regions of the relatively highest temperature near the reactor wall and the lowest temperature at the center of the reactor due to the natural endothermic behavior of the GSR process. Moreover, near the entrance of reactor, all foam sizes had a temperature change more than the 1-inch pellet. Among all foam sizes, the 30PPI foam catalyst showed the region of minimum temperature closely to the entrance length more than other sizes and the 10PPI foam catalyst showed the farthest length.
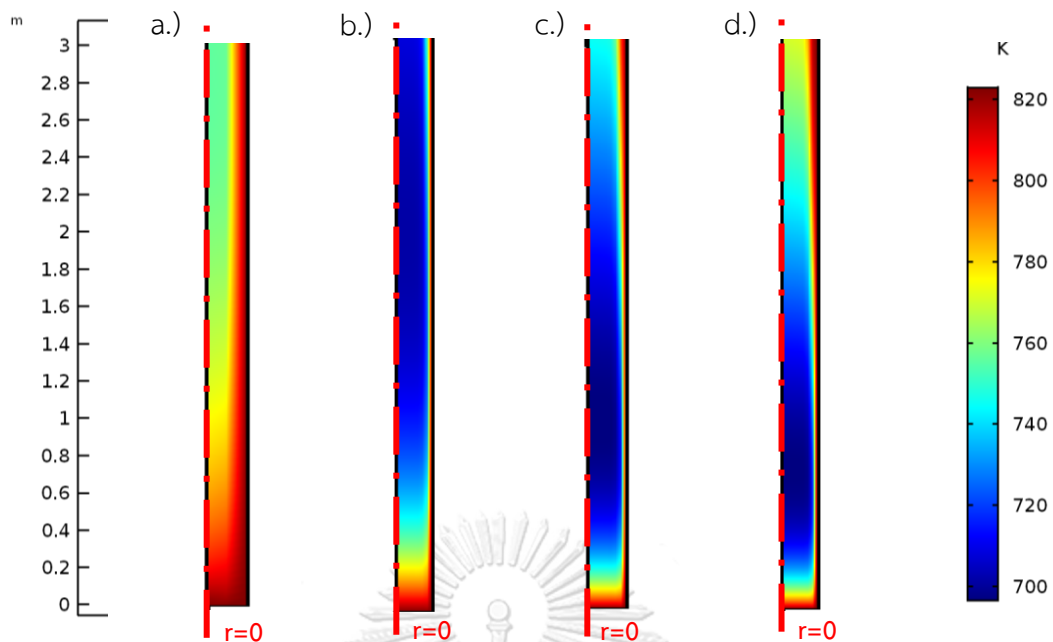
Figure 4.8 The temperature contour of 2D-symmetric reactor at the first 3 m length
a.) 1-inch pellet, b.) 10PPI foam, c.) 20PPI foam, and d.) 30PPI foam

Figure 4.9 showed the center temperature change along the reactor length of each catalyst structure. The reactor packed with the 1-inch pellet reached the minimum temperature of 755K at the early 20% of the reactor length; on the other hand, the temperature of all foam sizes drastically decreased from 823K to 700K in the early 7-10% of the reactor length. After this length, the temperature of both catalyst structures increased until constant at the inlet temperature of 823K. From the results, the magnitude of minimum temperature near the entrance length depended on the catalyst structures, wherein all foam sizes provided the lowest value compared to the 1-inch pellet. The feature of the external catalyst surface area influences to the reaction area and affects to the temperature change inside the reactor. The 30PPI foam catalyst with the greatest external catalyst surface area provided the minimum temperature of 696.71 K at 0.73 m length, while the 1-inch pellet catalyst with the lowest external catalyst surface area provided the minimum temperature of 755.65 K at 2.84 m length.
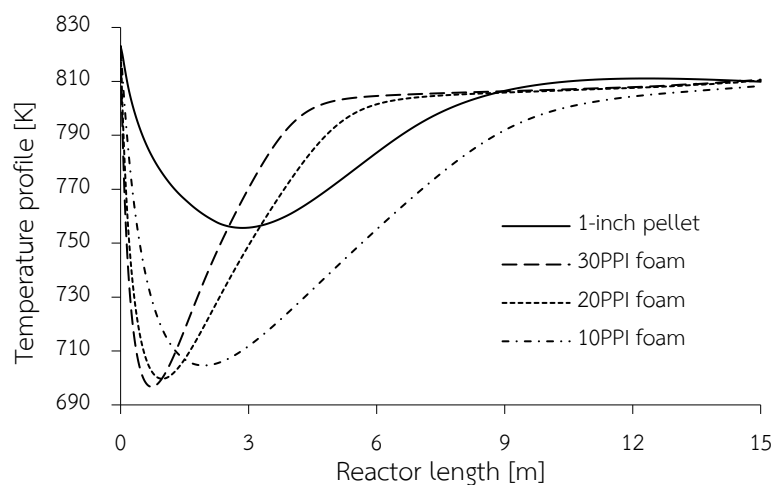
Figure 4.9 Temperature profile along the reactor length

The temperature dropping at the entrance length occurred from the endothermic main reaction of the GSR process that required heat to driving the reaction. Moreover, the side reaction of the GSR process is also considered in the simulation. As explained in Chapter 2.2, the GSR process composes of the glycerol decomposition, water-gas shift, and CO-methanation reaction, whereas each reaction presents with different behaviors. At the entrance length, the glycerol decomposition reaction acted as a main reaction and drawn the temperature dropping due to the endothermic behavior. After that, the product gases are generated and reduced the glycerol amount. The side reactions of the water-gas shift and the CO-methanation reaction will take place and increasing the temperature. In order to consider the contrast between the 1-inch pellet and the 30PPI foam, the 30PPI foam case provided more temperature dropping than the 1-inch pellet case because its larger surface area increased the reacting area and provided more product gases. Wherein the results of temperature change in this section corresponded to the results of glycerol conversion in section 4.3.2.

4.3.2 Chemical profile

- **Glycerol conversion**

The glycerol conversion is shown in Figure 4.10. At the entrance reactor, the glycerol conversion of both catalyst structures rapidly raised, then the glycerol conversion slowly increased after almost reaching 99% conversion. In order to compare the reactor length at 99% glycerol conversion of each catalyst structure, the reactor packed with the 1-inch pellet catalyst gave 99% conversion at 15 m of the reactor length, while the 10PPI, 20PPI, and 30PPI foam catalyst achieved at only 9.78, 4.93, and 3.71 m of the reactor length, respectively.
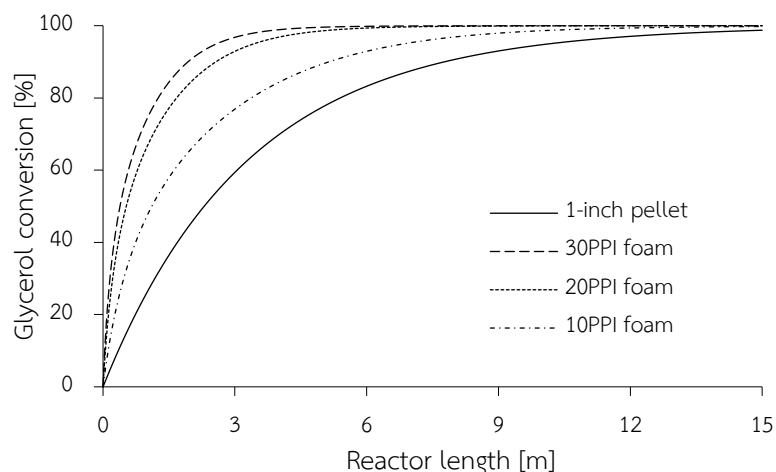
Figure 4.10 Glycerol conversion along the reactor length

The different results depended on their catalyst characteristic structures of the external surface area and the open porosity. As explained in section 4.2, the 30PPI foam catalyst gave 13 times higher of the external surface area than the 1-inch pellet catalyst. The larger external surface area and open porosity increases the prospective interaction between the reactants and the catalyst and provides more reaction spaces. Moreover, the higher porosity of the 30PPI foam also allows the convenient accessing of the reactants in the void area of the reactor.

In order to consider a reaction half-life of both catalyst structures, the 10PPI, 20PPI, and 30PPI foam catalyst gave only 0.4, 0.52, and 1.1 m of the reactor length, respectively, while the 1-inch pellet gave 2.3 m of the reactor length to decrease the glycerol concentration by half compared to the initial concentration, as shown in Figure 4.11. These results are also affected from the open-cell structure of the foam catalyst.
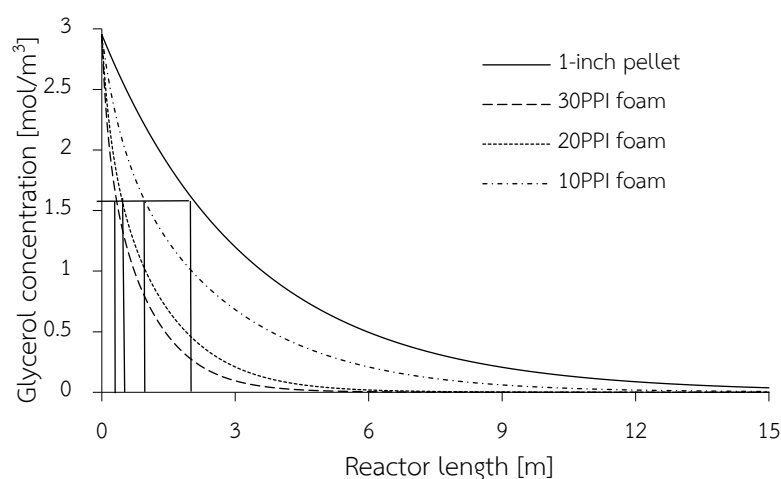
Figure 4.11 Glycerol concentration along the reactor length

- **Hydrogen yield**

The hydrogen yield of both catalyst structures is presented in Figure 4.12. The reactor packed with the 1-inch pellet catalyst gave the highest hydrogen yield of 56% at 15 m reactor length, while the reactor packed with the foam catalyst offered highest hydrogen yield of 60%. Although all foam sizes presented the same value of highest hydrogen yields, shooting points to achieve this highest hydrogen yield are differently. The shooting point of the 10PPI, 20PPI, and 30PPI foam are 5.56, 3.02, and 2.33m, respectively. After reaching the highest value, the hydrogen yield of all foam sizes slightly decreased and constant at 56% hydrogen yield, wherein the decreasing of hydrogen yield occurred from the shifting between the side reactions of the GSR process.

The results of hydrogen yield are corresponded to the results of glycerol conversion as explained above. But the results in the foam catalyst case presented a different behavior with the shooting point of maximum hydrogen yield. At this point, the glycerol conversion nearly completed, and the main reaction had been shifted from the glycerol decomposition reaction to other side reactions. The side reaction will change hydrogen to be the reactant and producing other undesired products of carbon monoxide, carbon dioxide, and methane.
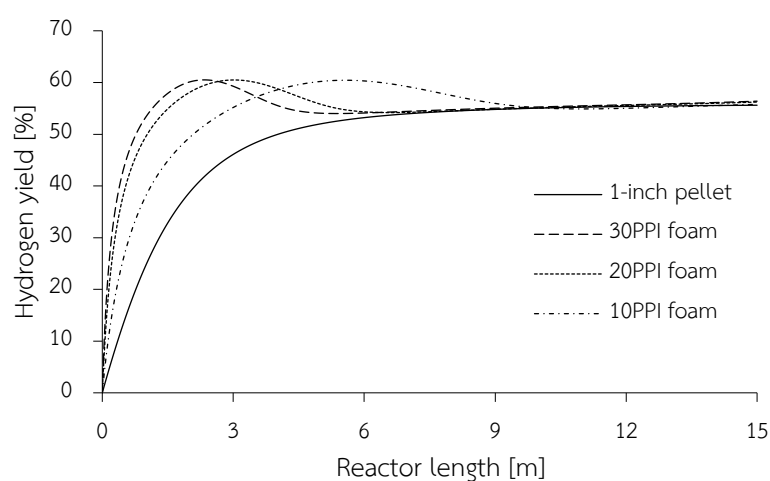
Figure 4.12 Hydrogen yield along the reactor length

- **Components distribution**

From the simulation, the concentration contour of each component is created and shown in Figure C3-C8 of Appendix C. But in chemical processing, the component flow rate must be presented to compare the quantity of components. The mole flow rates of all components in the GSR process are shown in Figure 4.13. The components of reactants (i.e., glycerol, and water) decreased along the reactor length, while the components of products (i.e., hydrogen, carbon dioxide, carbon monoxide, and methane) increased along the reactor length. At the entrance length, the reaction rapidly reacted to produce the product components from the reactants then the reaction gradually stabilized because the limiting reactant (glycerol) run out. At the outlet 15 m length, the reaction reached an equilibrium, and all catalyst structures

provided the same component mole flow rate but had a little deviation for water and methane.

At the shooting point of the foam catalyst, the productivity of all products (include desired and undesired products) is larger than the 1-inch pellet case because of the open-cell structure effect. Although the open-cell structure increased the desired product (H_2), the undesired products (CO_2, CO, CH_4) are also more occurred and affected to the purity of the desired product.

Because each catalyst structures had similar results of the component distribution at the outlet 15 m reactor length, the purity of components at the maximum hydrogen yield was considered instead. As shown in Table 4.3, the 30PPI foam catalyst showed the shortest reactor length to achieve the maximum hydrogen yield and the 1-inch pellet catalyst used the longest reactor length. In comparison, all foam sizes presented similar results of the components mole fraction, but the length of the reactor was differently. From the results, the 10PPI foam catalyst used the longest length and the 30PPI foam catalyst used the shortest length. The results of the different values obtained from the different reaction areas of each foam size as explained in the section above. Moreover, among all catalyst structures, the hydrogen product that produced from the 10PPI foam catalyst was purer than other foam sizes because it's produced less undesired byproducts, while the 1-inch pellet catalyst produced more impurity components with the longest reactor length.
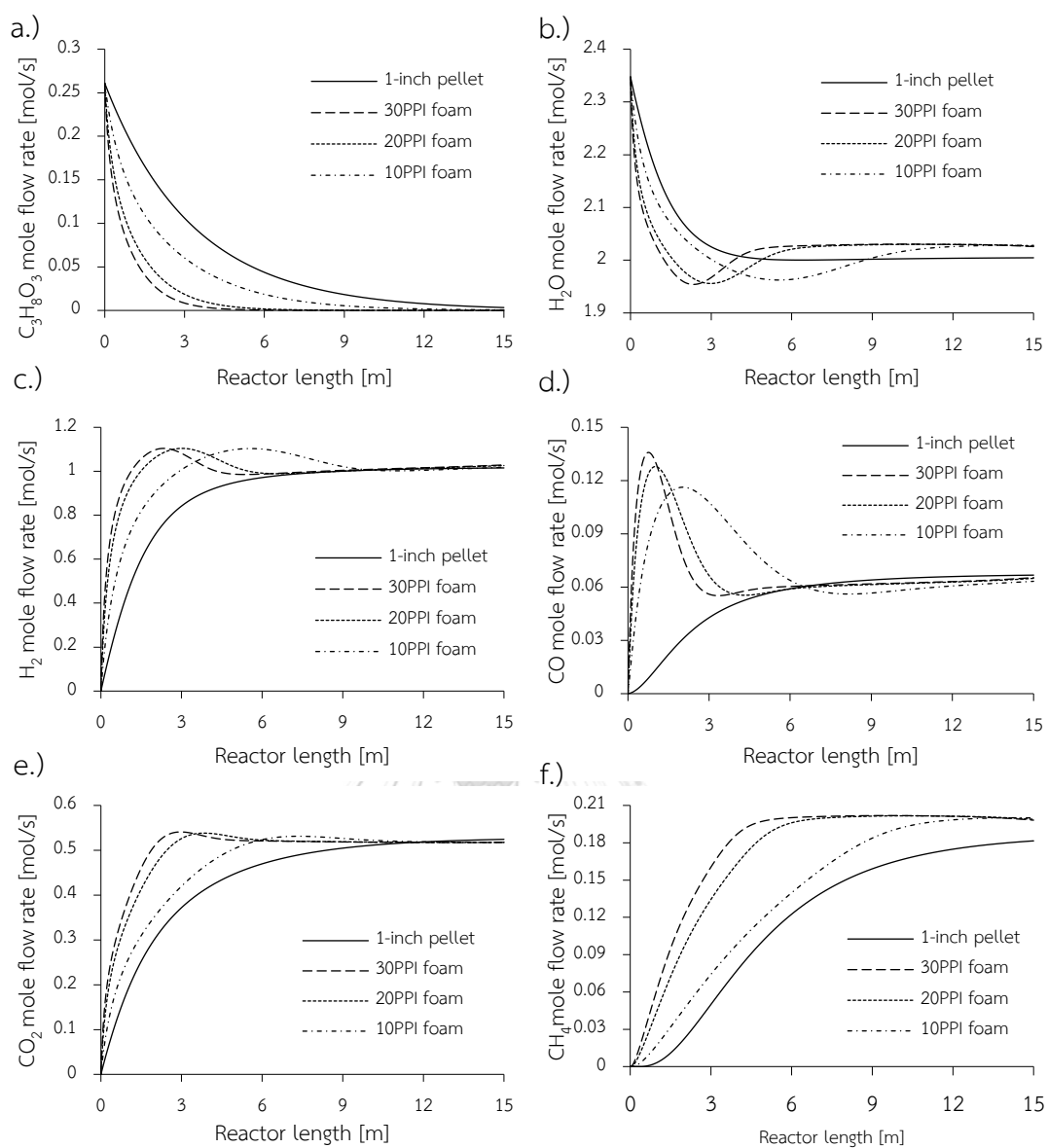
Figure 4.13 Mole flow rate of all components along the reactor length

a.) $C_3H_8O_3$, b.) H_2O, c.) H_2, d.) CO, e.) CO_2, and f.) CH_4

Table 4.3 Mole fraction of components at the maximum hydrogen yield

Mole fraction	1-inch pellet	10PPI foam	20PPI foam	30PPI foam
L	15	5.563	3.017	2.332
$C_3H_8O_3$	0	0.005	0.005	0.004
H_2O	0.527	0.515	0.514	0.513
H_2	0.267	0.290	0.290	0.290
CO	0.018	0.018	0.017	0.017
CO_2	0.139	0.136	0.138	0.139
CH_4	0.048	0.035	0.035	0.036
Total	0.999	0.999	0.999	0.999

4.4 Optimal design

After the results of the physical and chemical profile of each catalyst structure have been discussed in the section above, the summary of optimal catalyst structure inside the packed bed reactor must be specified to select the suitable catalyst structure of the GSR process. As presented in Table 4.4, the summarized table is shown the important parameters that performed the activity of catalyst with different size or construction on the reactor, for example, the open porosity (ε_0), the reactor length (L), a space-time yield (STY), the pressure drop (ΔP), and the maximum temperature difference (ΔT_{max}). From the table, the 1-inch pellet case gave the maximum hydrogen yield at 55.61%, while all foam sizes gave about 60.5% and using less reactor length. The effect of short reactor length provided the lower pressure drop that corresponding to a decreasing of the operating cost in the reactor. Moreover, one of the parameters to measure the activity of catalyst on the reactor with a different size or construction is the space-time yield (STY). The space-time yield is a parameter that exhibited the ratio between the quantity of desired product per unit weight of catalyst per unit time. In Table 4.3, the 1-inch pellet showed the STY at 11.80 $mol_{H2}/kg_{cat} \cdot hr$, while the 10PPI, 20PPI, and 30PPI foam are showed at 89.45, 142.81, and 163.33 $mol_{H2}/kg_{cat} \cdot hr$. The higher space time yield of all foam sizes performed the excellent catalyst activity more

than the 1-inch pellet catalyst because the open-cell structure of foam catalyst increased the amount of desired product (H_2) by using the lower catalyst weight.

Table 4.4 Summarized table of each catalyst structures at maximum hydrogen yield

Catalyst structure	ε_0	L	$Y_{H_2}^{max}$	STY	ΔP	ΔT_{max}
1-inch pellet catalyst	0.404	15	55.61	11.80	84.69	67.35
10PPI foam catalyst	0.87	5.56	60.44	89.45	2.04	118.37
20PPI foam catalyst	0.85	3.02	60.49	142.81	2.47	123.31
30PPI foam catalyst	0.83	2.33	60.51	163.33	3.34	126.29

From the above results, all foam sizes exhibited good results in both of physical and chemical profiles of the packed bed reactor in the GSR process. The foam catalyst performed the high value of space-time yield and hydrogen yield while using the lower catalyst weight, reactor length, and pressure drop. The use of foam catalyst instead of the pellet catalyst is one of the good choices to improve reactor performance.

Moreover, the 10PPI, 20PPI, and 30PPI foam catalysts are also investigated to evaluate the potential of foam sizes on the reactor performance by regarding the ratio between the hydrogen yield (desired product amount) and the pressure drop (operating cost), as shown in Figure 4.14. According to the summary results in Table 4.4, the 30PPI foam showed the maximum hydrogen yield at the shortest reactor length at 2.33 m. At this length, the results of each foam sizes are normalized with the corresponding results of the 30PPI catalyst for representing the relative results.

As shown in Figure 4.14 a.) and b.), the 10PPI foam presented the lowest value of normalized pressure drop and hydrogen yield, while the 30PPI foam presented the highest value comparing at the same reactor length. Furthermore, the ratio of normalized hydrogen yield to pressure drop was considered to assess the overall performance between the product and operation. In Figure 4.14 c.), the 10PPI foam had about three and two times more ratio than the 30PPI and 20PPI foam, respectively.

From the results, the 10PPI foam catalyst exhibited a better representation among all catalyst structures because this size reduced about 80% of the operating cost from the pressure drop by decreasing only 15% of product amount when compared with the 30PPI foam catalyst.
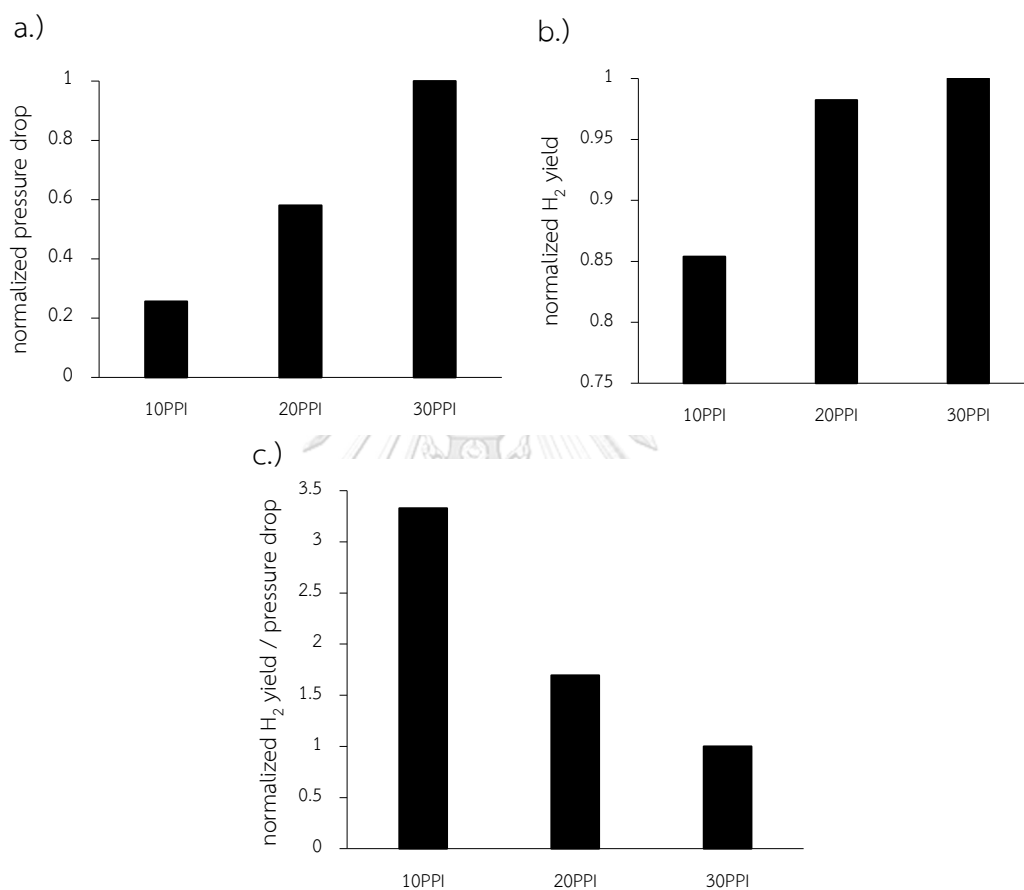

Figure 4.14 Normalized comparison of the foam sizes at 2.33 reactor length
a.) normalized pressure drop, b.) normalized hydrogen yield, and
c.) normalized hydrogen yield per unit pressure drop

CHAPTER 5 CONCLUSION AND RECOMMENDATIONS

5.1 Conclusion

To study the hydrogen production performances of the GSR process in the industrial-scale packed bed reactor. The different catalyst structures of the conventional pellet catalyst (1-inch spherical shape) and the novel foam catalyst (10-30PPI) were simulated via CFD simulation to compare their process performances.

From CFD results, all-foam catalyst cases offered the better results of pressure drop, glycerol conversion, and hydrogen yield than the conventional 1-inch pellet catalyst case. In the pressure drop section, the open-cell structure with the high open porosity of foam catalyst reduced more than five times of the pressure drop by compared with the 1-inch pellet catalyst. The lower pressure drop of the foam catalyst reduced the operating cost of the pump working in the reactor. Moreover, the open-cell structure of the foam catalyst also increased the external catalyst surface that multiplied up the prospective interaction between the reactants and the catalysts and provided more reaction spaces. According to the large external catalyst surface area of the foam catalyst, the maximum values of glycerol conversion and hydrogen yield can achieve at a shorter reactor length than the 1-inch pellet catalyst case. Moreover, the maximum temperature difference of the foam catalyst exhibited two times higher than the conventional 1-inch pellet catalyst. The greater temperature dropping indicated the high catalytic activity of the novel foam catalyst.

Furthermore, among 10PPI, 20PPI, and 30PPI foam catalysts, the 10PPI foam catalyst provided the better results more than other foam sizes. The 10PPI foam catalyst showed a lower normalized pressure drop and hydrogen yield about 80% and 15% than the 30PPI foam catalyst, respectively. This result showed the important action of the open porosity on the process performance. The 10PPI foam catalyst with highest open porosity provided similar product amount while using the lowest pressure drop.

From the study, the simulation results of the different catalyst structures in the GSR process confirmed better results of using the novel foam catalyst instead of the conventional pellet catalyst because the open-cell structure of the foam catalyst can eliminate the diffusion-limited behavior and the large pressure drop that is observed in the conventional pellet catalyst. Moreover, the reactor packed with the novel foam catalyst can produce more hydrogen by using a shorter reactor length than the conventional pellet catalyst. For all these reasons, the use of the novel foam catalyst structure can improve the hydrogen production of the GSR process and be favored in the packed bed reactor.

5.2 Recommendations

1. Including the reaction of the coke formation in the kinetic rate, because it was neglected in the study.

2. Developing the pseudo-homogeneous model to heterogeneous model, because the pseudo-homogeneous model has limited accuracy and did not present the appearance in catalyst scale.

3. Further study other operating condition of the GSR process in various foam sizes to study the effect of operating condition on the foam catalyst.

4. Varying the reactor size of each catalyst to study the variation of momentum, heat, and mass transfer inside the packed bed reactor.

REFERENCES

1. Program, U.S.G.C.R. *Global Climate Change Impacts in the United States*. 2009; Available from: https://climate.nasa.gov/causes/.

2. Balat, M., *Possible Methods for Hydrogen Production.* Energy Sources, Part A: Recovery, Utilization, and Environmental Effects, 2008. **31**(1): p. 39-50.

3. Acar, C. and Dincer, I., *Review and evaluation of hydrogen production options for better environment.* Journal of Cleaner Production, 2019. **218**: p. 835-849.

4. Li, D., Li, X. and Gong, J., *Catalytic Reforming of Oxygenates: State of the Art and Future Prospects.* Chemical Reviews, 2016. **116**(19): p. 11529-11653.

5. Chompupun, T., Limtrakul, S., Vatanatham, T., Kanhari, C. and Ramachandran, P.A., *Experiments, modeling and scaling-up of membrane reactors for hydrogen production via steam methane reforming.* Chemical Engineering and Processing - Process Intensification, 2018. **134**: p. 124-140.

6. Chen, J., Yan, L., Song, W. and Xu, D., *Comparisons between methane and methanol steam reforming in thermally integrated microchannel reactors for hydrogen production: A computational fluid dynamics study.* International Journal of Hydrogen Energy, 2018. **43**(31): p. 14710-14728.

7. Ma, R., Castro-Dominguez, B., Dixon, A.G. and Ma, Y.H., *CFD study of heat and mass transfer in ethanol steam reforming in a catalytic membrane reactor.* International Journal of Hydrogen Energy, 2018. **43**(15): p. 7662-7674.

8. Elewuwa, F.A. and Makkawi, Y.T., *Hydrogen production by steam reforming of DME in a large scale CFB reactor. Part I: Computational model and predictions.* International Journal of Hydrogen Energy, 2015. **40**(46): p. 15865-15876.

9. Silva, J.M., Soria, M.A. and Madeira, L.M., *Steam reforming of glycerol for hydrogen production: Modeling study.* International Journal of Hydrogen Energy, 2016. **41**(3): p. 1408-1418.

10. Dou, B., Song, Y., Wang, C., Chen, H. and Xu, Y., *Hydrogen production from catalytic steam reforming of biodiesel byproduct glycerol: Issues and challenges.* Renewable and Sustainable Energy Reviews, 2014. **30**: p. 950-960.

11. Bagnato, G., Iulianelli, A., Sanna, A. and Basile, A., *Glycerol Production and Transformation: A Critical Review with Particular Emphasis on Glycerol Reforming Reaction for Producing Hydrogen in Conventional and Membrane Reactors.* Membranes, 2017. **7**.

12. Schwengber, C.A., Alves, H.J., Schaffner, R.A., Silva, F.A.d., Sequinel, R., Bach, V.R., and Ferracin, R.J., *Overview of glycerol reforming for hydrogen production.* Renewable and Sustainable Energy Reviews, 2016. **58**: p. 259-266.

13. Palma, V., Ricca, A., Meloni, E., Martino, M., Miccio, M. and Ciambelli, P., *Experimental and numerical investigations on structured catalysts for methane steam reforming intensification.* Journal of Cleaner Production, 2016. **111**: p. 217-230.

14. Ghasemzadeh, K., Ghahremani, M., Amiri, T.Y. and Basile, A., *Performance evaluation of Pd-Ag membrane reactor in glycerol steam reforming process: Development of the CFD model.* International Journal of Hydrogen Energy, 2019. **44**(2): p. 1000-1009.

15. Wang, S., Yang, X., Xu, S. and Li, B., *Investigation into enhancing reforming of biomass-derived glycerol in a membrane reactor with hydrogen separation.* Fuel Processing Technology, 2018. **178**: p. 283-292.

16. Charoensuk, V., Bumroongsakulsawat, P., Assabumrungrat, S., Praserthdam, P. and Lohsoontorn, P.K., *Effect of the shape of catalyst freely falling by the gravity force in packed bed reactor on performance of glycerol steam reforming for hydrogen production.* 2019.

17. Wehinger, G.D., Kolaczkowski, S.T., Schmalhorst, L., Beton, D. and Torkuhl, L., *Modeling fixed-bed reactors from metal-foam pellets with detailed CFD.* Chemical Engineering Journal, 2019. **373**: p. 709-719.

18. Dixon, A.G., Nijemeisland, M. and Stitt, H., *CFD Simulation of Reaction and Heat Transfer Near theWall of a Fixed Bed.* INTERNATIONAL JOURNAL OF CHEMICAL REACTOR ENGINEERING, 2003. **1**.

19. Sundari, R. and Vaidya, P.D., *Reaction Kinetics of Glycerol Steam Reforming Using a Ru/Al$_2$O$_3$ Catalyst.* Energy Fuels, 2012. **26**: p. 4195-4204.

20. Nob Hill Publishing, L., *Fixed-Bed Catalytic Reactors*. 2018. p. 1-160.

21. Abe, I., *Physical and Chemical Properties of Hydrogen.* Encyclopedia of Life Support Systems (EOLSS); ENERGY CARRIERS AND CONVERSION SYSTEMS. **1**: p. 1-5.

22. Planete-Energies. *The Many Uses of Hydrogen*. 2015; Available from: https://www.planete-energies.com/en/medias/close/many-uses-hydrogen.

23. Information, N.C.f.B., *PubChem Compound Summary for CID 753, Glycerol.* PubChem, 2020.

24. ChemicalBook. *Glycerol*. 2015; Available from: https://www.chemicalbook.com/ChemicalProductProperty_EN_CB5339206.htm.

25. Chiodo, V., Freni, S., Galvagno, A., Mondello, N. and Frusteri, F., *Catalytic features of Rh and Ni supported catalysts in the steam reforming of glycerol to produce hydrogen.* Applied Catalysis A: General, 2010. **381**(1): p. 1-7.

26. Abbas, S.Z., Dupont, V. and Mahmud, T., *Kinetics study and modelling of steam methane reforming process over a NiO/Al2O3 catalyst in an adiabatic packed bed reactor.* International Journal of Hydrogen Energy, 2017. **42**(5): p. 2889-2903.

27. Avasthi, K.S., Reddy, R.N. and Patel, S., *Challenges in the Production of Hydrogen from Glycerol – A Biodiesel Byproduct Via Steam Reforming Process.* Procedia Engineering, 2013. **51**: p. 423-429.

28. Wang, X., Wang, N., Li, M., Li, S., Wang, S. and Ma, X., *Hydrogen production by glycerol steam reforming with in situ hydrogen separation: A thermodynamic investigation.* International Journal of Hydrogen Energy, 2010. **35**(19): p. 10252-10256.

29. Klaewkla, R., Arend, M. and Hoelderich, W.F., *A Review of Mass Transfer Controlling the Reaction Rate in Heterogeneous Catalytic Systems*, ed. M.T.-A. Aspects. 2011: InTech.

30. Fogler, H.S., *Essentials of Chemical Reaction Engineering*. 2010: Prentice Hall International Series in the Physical and Chemical Engineering Sciences.

31. Bakker, A., Haidari, A. and Marshall, E.M., *Design reactors via CFD.* Chemical Engineering Progress, 2001. **97**: p. 30-39.

32. Twigg, M. and Richardson, J., *Fundamentals and Applications of Structured Ceramic Foam Catalysts.* Industrial & Engineering Chemistry Research - IND ENG CHEM RES, 2007. **46**.

33. Adhikari, S., Fernando, S. and Haryanto, A., *Kinetics and Reactor Modeling of Hydrogen Production from Glycerol via Steam Reforming Process over Ni/CeO2 Catalysts.* Chemical Engineering & Technology, 2009. **32**: p. 541-547.

34. Cheng, C.K., Foo, S.Y. and Adesina, A.A., *Glycerol Steam Reforming over Bimetallic Co–Ni/Al2O3.* Ind. Eng. Chem. Res., 2010. **49**(21): p. 10804-10817.

35. Shahirah, M.N.N., Abdullah, S., Gimbun, J., Ng, Y.H. and Cheng, C.K., *A study on the kinetics of syngas production from glycerol over alumina-supported samarium–nickel catalyst.* International Journal of Hydrogen Energy, 2016. **41**(25): p. 10568-10577.

36. Multiphysics, C. *Understand, Predict, and Optimize Physics-Based Designs and Processes with COMSOL Multiphysics®.* 2020; Available from: https://www.comsol.com/comsol-multiphysics.

37. Anderson, J.D., *Computational Fluid Dynamics: The Basics With Applications. Science/Engineering/Math.* 1995: McGraw-Hill Science.

38. Fuller, E.N., Schettler, P.D. and Giddings, J.C., *NEW METHOD FOR PREDICTION OF BINARY GAS-PHASE DIFFUSION COEFFICIENTS.* Industrial & Engineering Chemistry, 1966. **58**(5): p. 18-27.

39. Liu, G.R. and Quek, S.S., *The Finite Element Method: A Practical Course*. 2003: Elsevier Science.

40. Wikipedia, *Newton's method*. 2020: Wikipedia.

41. KRITTACOM, B., *NUMERICAL METHOD FOR ENGINEERING*. 252.

42. Ru ́a, D. and Herna ́ndez, L., *Phenomenological evaluation of industrial reformers for glycerol steam reforming.* Hydrogen Energy, 2016. **41**: p. 13811-13819.

43. Kent, J.E., *Steam Reforming of Biodiesel By-Product Glycerol*. 2013, WORCESTER POLYTECHNIC INSTITUTE. p. 1-81.

44.   Gancarczyk, A., Sindera, K., Iwaniszyn, M., Piatek, M., Macek, W., Jodłowski, P.J., Wro'nski, S., Sitarz, M., Łojewska, J., and Kołodziej, A., *Metal Foams as Novel Catalyst Support in Environmental Processes.* catalysts, 2019. **9**(587): p. 1-13.

45.   Palma, V., Pisano, D. and Martino, M., *CFD modeling of the influence of carrier thermal conductivity for structured catalysts in the WGS reaction.* Chemical Engineering Science, 2018. **178**.

46.   Ergun, S., *Fluid flow through packed columns.* Chemical Engineering Process, 1952. **48**(2): p. 89-94.

47.   Inayat, A., Klumpp, M., Lämmermann, M., Freund, H. and Schwieger, W., *Development of a new pressure drop correlation for open-cell foams based completely on theoretical grounds: Taking into account strut shape and geometric tortuosity.* Chemical Engineering Journal, 2016: p. 1-44.

48.   MacDonald, B. and Olm, A., *Reaction and Transport in Industrial-Scale Packed Bed Steam Reforming of Glycerol*, in *Chemical Engineering*. 2014, WORCESTER POLYTECHNIC INSTITUTE. p. 89.

จุฬาลงกรณ์มหาวิทยาลัย
CHULALONGKORN UNIVERSITY

ABBREVIATIONS

Symbol	Description	Unit
C_F	Forchheimer-coefficient	m
$C_{P,f}$	Fluid (mixture) specific heat capacity	J/kg·K
C_i	Molar concentration of species i	mol/m^3
d_p	Spherical pellet catalyst diameter	m
d_{por}	Particle pore diameter	m
d_h	Hydraulic diameter	m
d_s	Strut diameter	m
$D_{eff,i}$	Effective diffusion coefficient	m^2/s
$D_{KA,i}$	Knudsen diffusivity	m^2/s
D_{ik}	Binary diffusion coefficient of species i and k	m^2/s
D_i^m	Diffusion coefficient of species i in a mixture	m^2/s
Ea_j	Activation energy of reaction j	kJ/mol
J_i	Molar diffusion flux of species i	mol/m^{2}s
k_{rxn}	Reaction constant	-
k_j	Kinetic rate constant of reaction j	depends
$k_{0,j}$	Pre-exponential factor of reaction j	depends
K	Permeability	m^2
K_i	Adsorption constant of species i	depends
$K_{0,i}$	Reference adsorption constant of species i	depends
K_j	Thermodynamic equilibrium constant of reaction j	-
L_{re}	Reactor length	m
Mw_i	Molecular weight of species i	kg/kmol
n	Order of reaction	-
p_i	Partial pressure of species i	Pa

Symbol	Description	Unit
P	Pressure	Pa
q	Heat flux	W/m^2
Q_{sv}	External heat source	W/m^2
r	Radian coordinate	m
R	Gas constant	J/mol·K
R_{re}	Reactor radian	m
R_j	Rate of reaction j	mol/m^2s
S_v	Geometric surface area of catalyst per unit volume reactor	m^2/m^3
STY	Space-time yield	mol_{H2}/kg_{cat}·hr
t	Time	s
T	Temperature	K
u	Velocity	m/s
y_i	Mole fraction of species i	-
Y_{H2}	Hydrogen yield	%
z	Axial coordinate	m
Greek		
∇	divergence	-
ΔH_j	Reaction enthalpy of reaction j	kJ/mol
ΔH_i	Heat of adsorption of species i	kJ/mol
β	Partial reaction order of glycerol	-
γ	Partial reaction order of steam	-
ε_p	Catalyst particle porosity	-
ε_o	open porosity	-
Ω	Unit less adsorption factor	-
τ_{stress}	Shear stress	Pa
τ	Tortuosity	-

Symbol	Description	Unit
ρ_{bulk}	Reactor bed density	kg/m^3
ρ_{cat}	Catalyst density	kg/m^3
ρ_f	Fluid (mixture) density	kg/m^3
υ_{ij}	Stoichiometric coefficient of species I in reaction j	-
μ_f	Fluid (mixture) viscosity	Pa·s
θ	Angular coordinate	°
δ	Tensor unit	-
$\sum v_i$	Sum of the diffusion volume of component	-

Abbreviations

CFD	Computational fluid dynamic	
GSR	Glycerol steam reforming	
PDEs	Partial differential equations	
PPI	Pore per inch	
WGFR	Steam to glycerol feed ratio (mole basis)	

จุฬาลงกรณ์มหาวิทยาลัย

CHULALONGKORN UNIVERSITY

APPENDIX A: **Details of model validation**

Table A1 Characteristics of reactor from Macdonald, Bryan et al., (2014) [48]

Parameters	Values
Reactor length (m)	4
Reactor diameter (m)	0.15
Spherical catalyst diameter (m)	0.0254
Catalyst density (kg/m^3)	1947
Porosity of bed (-)	0.4
Mass of catalyst (kg)	80

Table A2 Operating conditions from Macdonald, Bryan et al., (2014) [48]

Parameters	Values
Temperature (K)	823
Pressure (Pa)	2.02×10^5
Steam to glycerol ratio (mole basis)	9:1
Linear velocity (m/s)	5

APPENDIX B: Diffusion coefficient

The diffusion coefficient is a parameter to describe the transport of mass in gas, liquid, and solid phase under the influence of a concentration gradient. In the packed bed reactor, the main diffusion coefficient parameter is separated into 2 phases of gas and solid phase. In the gas phase, the Stefan-Maxwell diffusion equation with the characteristics of gas species (e.g. molecular weight, diffusion volume, and mole fraction) is used to describe the diffusion coefficient (D_i^F) of each species in a mixture, as shown in Eq. 2.23-2.24. In the solid phase, the relation between the molecular diffusion and the Knudsen diffusion with the characteristics of medium (e.g. particle porosity, tortuosity, and particle pore diameter) is used to describe the effective diffusion coefficient ($D_{eff,i}$), as shown in Eq. 2.25-2.26. The values of the diffusion

coefficient in Table B1 and B2 were calculated based on the operating condition in Table 9.

Table B1: The diffusion coefficient

Components	Molecular diffusivity (D_i^F)
$C_3H_8O_3$	4.73×10^{-5}
H_2	8.17×10^{-4}
CO	1.04×10^{-4}
H_2O	1.32×10^{-4}
CO_2	7.91×10^{-5}
CH_4	1.28×10^{-4}

Table B2: The effective diffusion coefficient

Components	Effective diffusivity ($D_{eff,i}$)			
	1-inch pellet	10PPI foam	20PPI foam	30PPI foam
$C_3H_8O_3$	4.62×10^{-7}	2.99×10^{-5}	2.88×10^{-5}	2.77×10^{-5}
H_2	3.28×10^{-6}	5.15×10^{-4}	4.96×10^{-4}	4.77×10^{-4}
CO	8.49×10^{-7}	6.56×10^{-5}	6.31×10^{-5}	6.08×10^{-5}
H_2O	1.06×10^{-6}	8.34×10^{-5}	8.03×10^{-5}	7.73×10^{-5}
CO_2	6.75×10^{-7}	4.99×10^{-5}	4.80×10^{-5}	4.62×10^{-5}
CH_4	1.12×10^{-6}	8.06×10^{-5}	7.76×10^{-5}	7.47×10^{-5}

APPENDIX C: CFD contour along the reactor length

According to the CFD simulation, pressure, temperature, and concentration contours of each catalyst structure have been created to present the variation of each parameter along the reactor length. The representation color is shown between the blue and red colour, where the blue color presented the lowest value, and the red color presented the highest value. each result of pressure, temperature, and concentration contours in Figure C1, C2, and C3-C8 are corresponded to the results in Figure 4.5, 4.9, and 4.13.
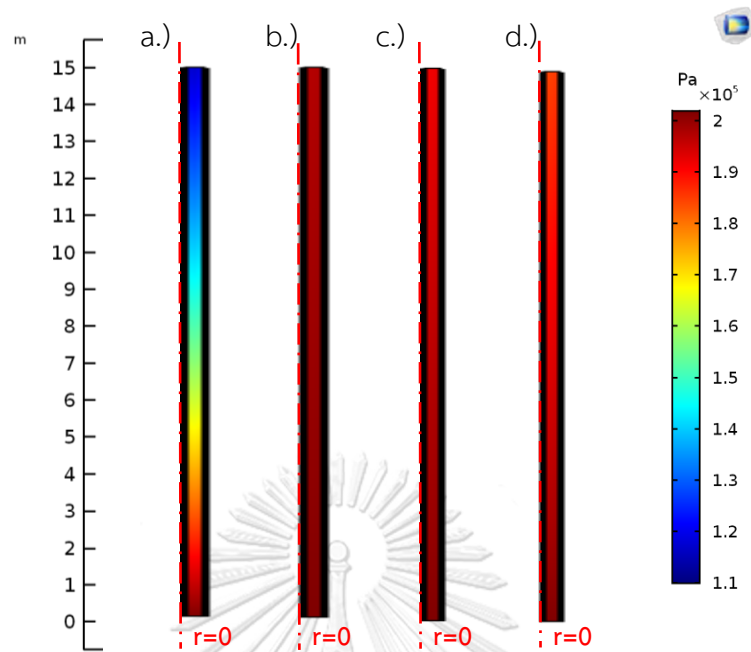
Figure C1 Pressure contour along the reactor length

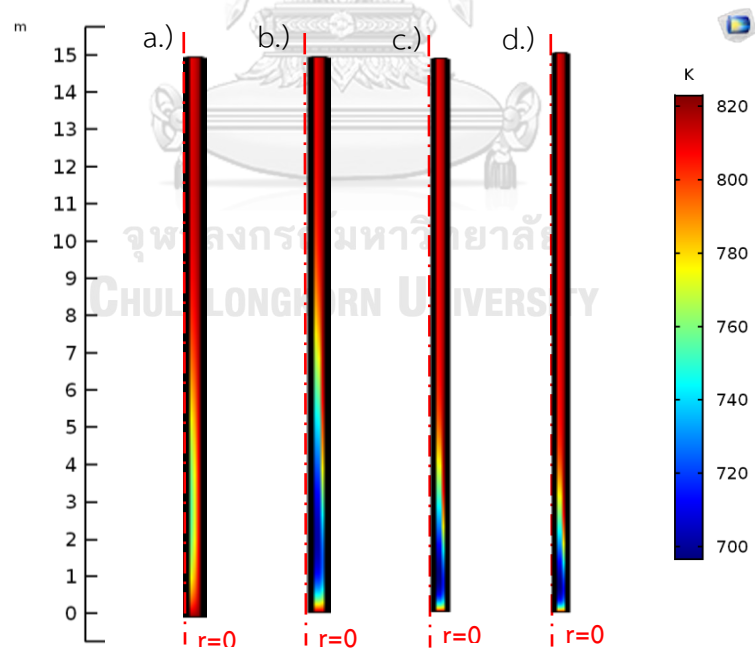a.) 1-inch pellet, b.) 10PPI foam, c.) 20PPI foam, and d.) 30PPI foam

Figure C2 Temperature contour along the reactor length

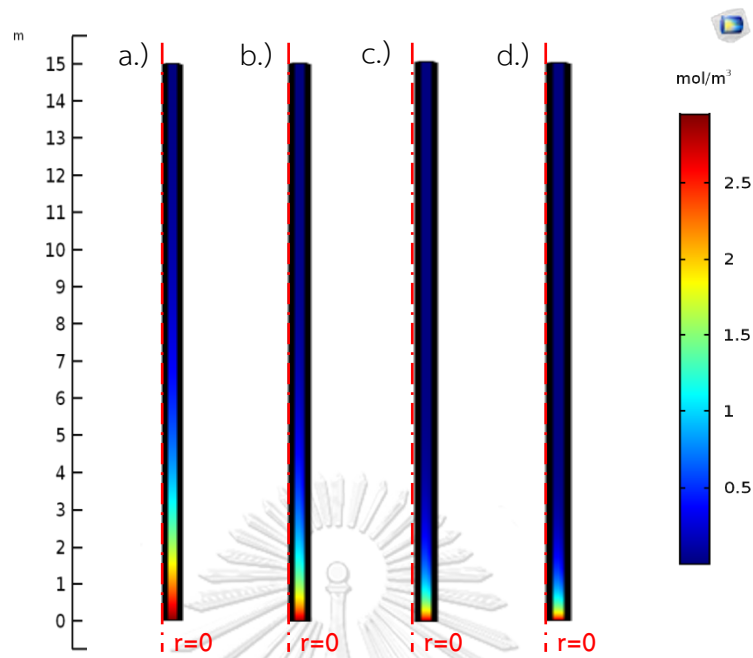a.) 1-inch pellet, b.) 10PPI foam, c.) 20PPI foam, and d.) 30PPI foam

Figure C3 $C_3H_8O_3$ concentration contour along the reactor length

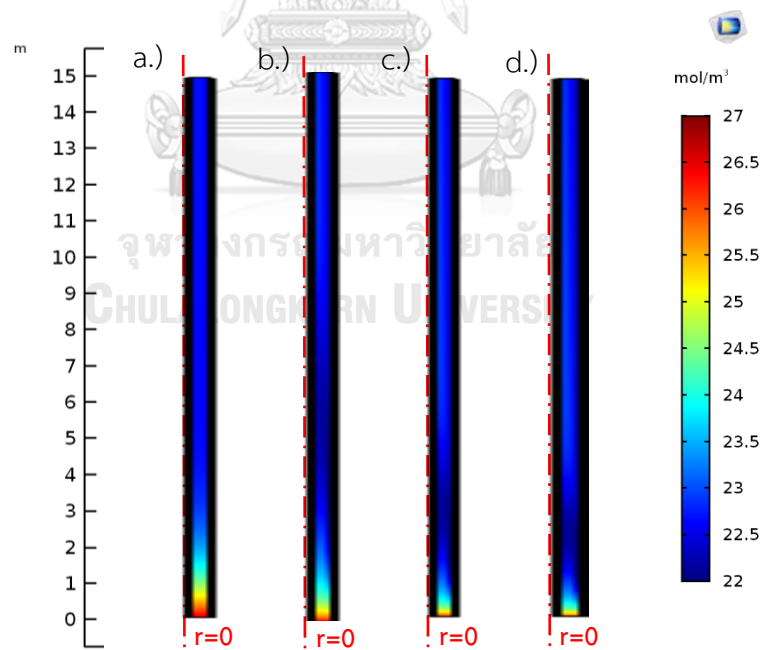a.) 1-inch pellet, b.) 10PPI foam, c.) 20PPI foam, and d.) 30PPI foam

Figure C4 H_2O concentration contour along the reactor length

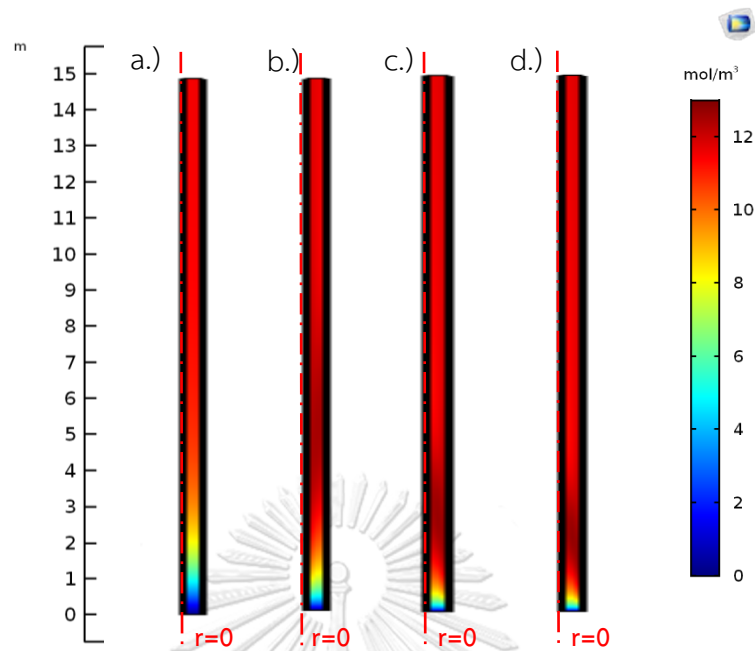a.) 1-inch pellet, b.) 10PPI foam, c.) 20PPI foam, and d.) 30PPI foam

Figure C5 H_2 concentration contour along the reactor length

a.) 1-inch pellet, b.) 10PPI foam, c.) 20PPI foam, and d.) 30PPI foam
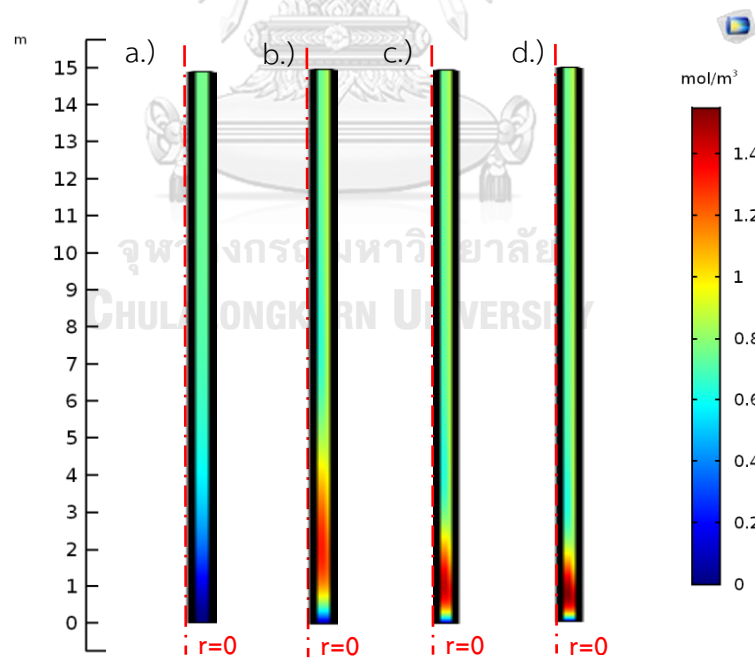

Figure C6 CO concentration contour along the reactor length

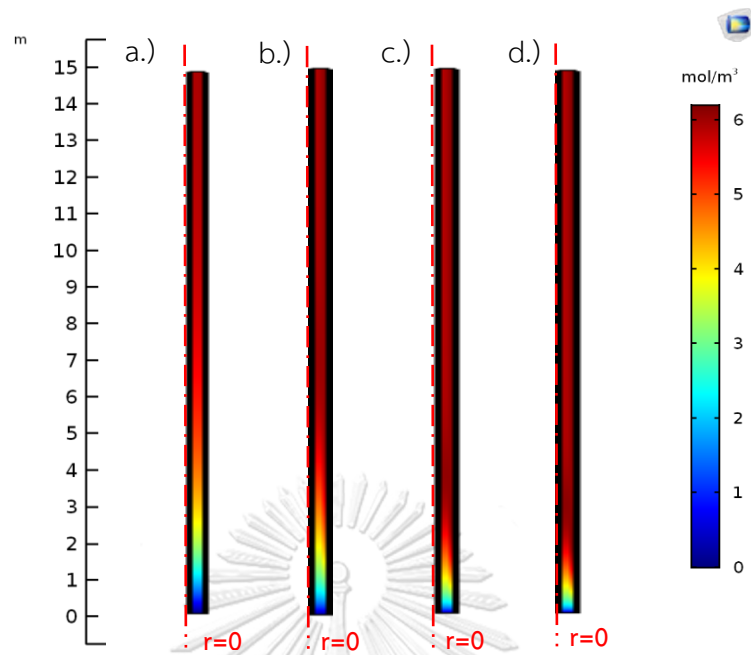a.) 1-inch pellet, b.) 10PPI foam, c.) 20PPI foam, and d.) 30PPI foam

Figure C7 CO_2 concentration contour along the reactor length

a.) 1-inch pellet, b.) 10PPI foam, c.) 20PPI foam, and d.) 30PPI foam

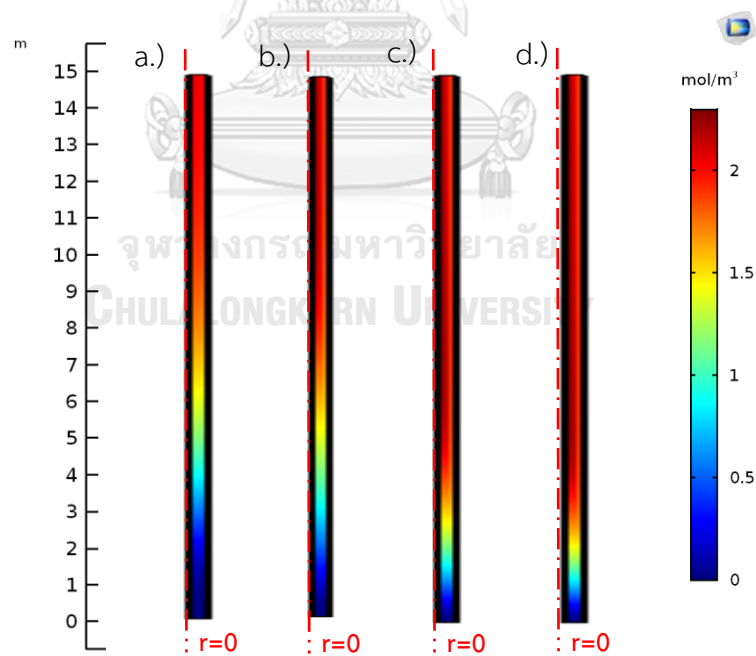Figure C8 CH_4 concentration contour along the reactor length

a.) 1-inch pellet, b.) 10PPI foam, c.) 20PPI foam, and d.) 30PPI foam

VITA

NAME   Miss Chattharika Phitchayakorn

DATE OF BIRTH   5 May 1994

INSTITUTIONS ATTENDED   King Mongkut's University of Technology North Bangkok